



**UNIVERSIDADE ESTADUAL DE CAMPINAS**  
**Faculdade de Engenharia Mecânica**

**Max William Frasão Reis**

*Study of boiling phenomenon using the droplet evaporation method*

*Estudo do fenômeno de ebulação usando o método de evaporação de gotículas*

CAMPINAS  
2019

**Max William Frasão Reis**

***Study of the boiling phenomenon using the  
droplet evaporation method***

***Estudo do fenômeno de ebulação usando o  
método de evaporação de gotículas***

Dissertation presented to the School of Mechanical Engineering of the University of Campinas in partial fulfillment of the requirements for the degree of Master in Mechanical Engineering, in the area of Thermal and Fluid Engineering.

Dissertação apresentada à Faculdade de Engenharia Mecânica da Universidade Estadual de Campinas como parte dos requisitos exigidos para obtenção do título de Mestre em Engenharia Mecânica, na Área de Térmica e Fluidos.

Orientador: Prof. Dr. Rogério Gonçalves dos Santos

ESTE EXEMPLAR CORRESPONDE À VER-  
SÃO FINAL DA DISSERTAÇÃO DEFENDIDA  
PELO ALUNO MAX WILLIAM FRASÃO REIS  
E ORIENTADO PELO PROF. DR ROGÉRIO  
GONÇALVES DOS SANTOS.

**CAMPINAS**  
**2019**

Ficha catalográfica  
Universidade Estadual de Campinas  
Biblioteca da Área de Engenharia e Arquitetura  
Rose Meire da Silva - CRB 8/5974

R277s Reis, Max William Frasão, 1993-  
Study of the boiling phenomenon using the droplet evaporation method /  
Max William Frasão Reis. – Campinas, SP : [s.n.], 2019.

Orientador: Rogério Gonçalves dos Santos.  
Dissertação (mestrado) – Universidade Estadual de Campinas, Faculdade  
de Engenharia Mecânica.

1. Combustíveis. 2. Evaporação. 3. Evaporação - Aplicações industriais. 4. Gotícula. 5. Ebulação. I. Santos, Rogério Gonçalves dos, 1978-. II. Universidade Estadual de Campinas. Faculdade de Engenharia Mecânica. III. Título.

Informações para Biblioteca Digital

**Título em outro idioma:** Estudo do fenômeno de ebulação usando o método de evaporação de gotículas

**Palavras-chave em inglês:**

Fuels

Evaporation

Evaporation - Industrial applications

Droplet

Boiling

**Área de concentração:** Térmica e Fluídos

**Titulação:** Mestre em Engenharia Mecânica

**Banca examinadora:**

Rogério Gonçalves dos Santos [Orientador]

Marcelo Souza de Castro

Gherhardt Ribatski

**Data de defesa:** 25-02-2019

**Programa de Pós-Graduação:** Engenharia Mecânica

**Identificação e informações acadêmicas do(a) aluno(a)**

- ORCID do autor: <https://orcid.org/0000-0002-3482-0854>

- Currículo Lattes do autor: <http://lattes.cnpq.br/5809501474561779>

**UNIVERSIDADE ESTADUAL DE CAMPINAS  
FACULDADE DE ENGENHARIA MECÂNICA  
COMISSÃO DE PÓS-GRADUAÇÃO EM ENGENHARIA MECÂNICA  
DEPARTAMENTO DE ENERGIA**

**DISSERTAÇÃO DE MESTRADO ACADÊMICO**

***Study of the boiling phenomenon using the  
droplet evaporation method***

***Estudo do fenômeno de ebulação usando o  
método de evaporação de gotículas***

Autor: Max William Frasão Reis

Orientador: Rogério Gonçalves dos Santos

A Banca Examinadora composta pelos membros abaixo aprovou esta Dissertação:

**Prof. Dr. Rogério Gonçalves dos Santos, Presidente  
Instituição UNICAMP/FEM**

**Prof. Dr. Marcelo Souza de Castro  
Instituição UNICAMP/FEM**

**Prof. Dr. Gherhardt Ribatski  
Instituição USP/EESC/SEM**

A Ata da defesa com as respectivas assinaturas dos membros encontra-se no processo de vida acadêmica do aluno.

Campinas, 25 de Fevereiro de 2019.

## **Dedication**

I dedicate this work to my parents who have always supported me, and to my friends who contributed to the realization this research.

## Agradecimentos

Apesar desta dissertação estar escrita em inglês, gostaria de expressar meus agradecimentos em minha língua materna.

Gostaria de agradecer primeiramente à Deus por sempre me ajudar nos momentos difíceis da minha vida e por ter me dado forças para continuar seguindo em frente até a conclusão do presente trabalho.

A minha família em especial meus pais Antonio José Costa Reis e Maria Irenilde Pereira Frazão Reis pela educação, incentivo, suporte pois apesar da distância sempre me ajudavam de todas as formas possíveis.

Meu sincero agradecimento ao Professor Rogério pela oportunidade de trabalhar em seu grupo de pesquisa. Não apenas pela orientação mas também pelo apoio, auxílio, paciência e incentivo durante todo mestrado. Ao professor Rogério eu só tenho à agradecer.

Ao Dr. Arthur Vieira que também fez parte deste projeto e colaborou significamente para o desenvolvimento desta pesquisa sempre dando o suporte necessário para que todas as etapas deste projeto fossem concluídas da melhor forma possível, e por todo conhecimento que adquiri ao longo de nossas reuniões na UNICAMP e na Magneti Marelli.

Queria agradecer também a Magneti Marelli Sistemas Automotivos pela construção da bancada e pelo suporte em outras etapas do projeto. Sem sua participação seria impossível a realização desta pesquisa.

Queria agradecer ao Fernando (técnico do Departamento de Mecânica Computacional) que sempre me ajudou na parte técnica da bancada quando possível.

Aos membros das banca de qualificação e defesa que contribuiram dando sugestões e fazendo críticas construtivas para melhoria desta pesquisa.

Aos amigos e companheiros que sempre estiveram do meu lado durante essa caminhada. Em especial ao George, Yuri, Brenno, Mavd, Lucas (D.M.C), Lucas (D.S.I), Taynara, Paulinho e Danilo. Sou grato a cada um de vocês.

Gostaria de agradecer em especial ao meu amigo Rayston que sempre me ajudou e me aconselhou de forma sábia durante nossa estadia em Campinas.

O presente trabalho foi realizado com apoio da Coordenação de Aperfeiçoamento de Pessoal de Nível Superior Brasil (CAPES) - Código de Financiamento 001.

*Success is born of want, determination, and persistence in reaching a goal. Even if you do not reach the target, those who seek and overcome obstacles will at least do wonderful things.*

---

José de Alencar

## **Resumo**

A ebulação é um dos mecanismos mais eficientes e com maiores taxas de transferência de calor. O estudo deste fenômeno é geralmente baseado em experimentos de grande complexidade, o que dificulta a identificação de parâmetros relevantes para aplicações práticas, como as temperaturas de Nukiyama e Leidenfrost. O objetivo desta pesquisa foi obter as temperaturas de Nukiyama e Leidenfrost a partir da evaporação de gotículas de diferentes fluidos em uma superfície aquecida e avaliar a influência do material da superfície e do número de Weber nestes pontos críticos. Os fluidos testados foram: água destilada, etanol, iso-octano, n-heptano e misturas de 11,1% etanol - 88,9% n-heptano, 65% etanol - 35% n-heptano e 90% etanol - 10% n-heptano, 10% etanol - 90% gasolina, 20% etanol - 80% gasolina, 35% etanol - 65% gasolina, 50% etanol - 50% gasolina, 65% etanol - 35% gasolina, 80% etanol - 20% gasolina, 90% etanol - 10% gasolina, respectivamente. Os resultados para componentes únicos foram comparados com valores encontrados através de correlações e dados experimentais de outros autores onde alguns resultados concordaram com dados da literatura e outros não. A temperatura de Leidenfrost para gasolina e algumas misturas gasolina - etanol não foi encontrada. Outros parâmetros foram avaliados como a influência da força da resistência do ar na gota e a radiação emitida pela superfície de aquecimento na temperatura da agulha.

*Palavras-chave:* Ebulação, Combustíveis, Evaporação de gota, Ponto de Nukiyama, Ponto de Leidenfrost.

## **Abstract**

Boiling is one of the most efficient mechanisms with the highest heat transfer rates. The study of this phenomenon is usually based on experiments of great complexity, which makes it difficult to identify parameters relevant to practical applications, such as Nukiyama and Leidenfrost temperatures. The objective of this research was to obtain the Nukiyama and Leidenfrost temperature from the Droplet evaporation of different fluids on a heated surface and to evaluate the influence of surface material and Weber number on these critical points. The fluids tested were: distilled water, ethanol, iso-octane, n-heptane and mixtures of 11.1% ethanol 88.9% n-heptane, 65% ethanol 35% n-heptane and 90% ethanol 10% ethanol, 10% ethanol - 90% gasoline, 20% ethanol - 80% gasoline, 35% ethanol - 65% gasoline, 50% ethanol - 50% gasoline, 65% ethanol - 35% gasoline, 80% ethanol - 20% gasoline, 90% ethanol - 10% gasoline, respectively. The results for single-components were compared with values found through correlations and experimental data of other authors where some results agreed with data from the literature and others did not. The Leidenfrost temperature for gasoline and some gasoline - ethanol blends was not found. Other parameters were evaluated as the influence of air resistance force on the droplet and the radiation emitted by the heating surface at the needle temperature.

*Keywords:* Boiling, Fuels, Droplet evaporation, Nukiyama point, Leidenfrost Point.

## List of Figures

2.1	Typical boiling (a) and droplet lifetime curve (b) with the critical points. . . . .	23
2.2	Vapor structure in nucleate boiling generated in cavity: discrete bubbles (a), vapor columns (b). . . . .	24
2.3	Illustration of a droplet in Leidenfrost regime. . . . .	26
2.4	Illustrated of system wetting. . . . .	30
2.5	Configurations of the solid-droplet interaction with surfaces: no-wetting (a), wetting (b), and totally wetting (c). . . . .	30
2.6	Depiction of advancing and receding contact angles. . . . .	31
2.7	Illustrated of the Gibbs energy curve for a real wetting system. . . . .	32
2.8	Main forces in the droplet impact on a heated surface. . . . .	33
2.9	Depiction of droplet impact regimes on a solid surface. . . . .	34
3.1	Detailed drawing of test bench in CAD. . . . .	36
3.2	Schematic drawing of the droplet evaporation process. . . . .	37
3.3	Pneumatic system. . . . .	38
3.4	Droplet generation mechanism. . . . .	38
3.5	Heating system details. . . . .	39
3.6	Temperature controller model 1030 (NOVUS company). . . . .	39
3.7	Test section with thermocouples. . . . .	40
3.8	Data acquisition system composed of a computer corporation and Fieldlogger of Novus company (adapted by author). . . . .	40
3.9	Recording and lighting system. . . . .	41
3.10	Complete apparatus experimental. . . . .	42
3.11	Test diagram. . . . .	43
3.12	Items used to prepare the mixtures. . . . .	44
3.13	Illustrative image of data acquisition dynamics. . . . .	45
3.14	Evaporation test of droplet at high acquisition rate with filter value variation ( $T_s = 130^\circ\text{C}$ ). . . . .	46
3.15	Evaporation test of drop at low acquisition rate with filter variation ( $T_s = 230^\circ\text{C}$ ). . . . .	47
3.16	Evaporation test of droplet in high acquisition rate in Leidenfrost point ( $T_s = 230^\circ\text{C}$ ). . . . .	47
3.17	Image of the thermocouple calibration process. . . . .	48
4.1	Frames taken from the test with n-Heptane: (a) at $125^\circ\text{C}$ ; (b) $180^\circ\text{C}$ . . . . .	49
4.2	Results of the droplet lifetime with the surface temperature for ethanol. . . . .	50
4.3	Results of the droplet lifetime with the surface temperature for Iso-Octane. . . . .	51
4.4	Results of the droplet lifetime with the surface temperature for n-Heptane. . . . .	51
4.5	Results of the droplet lifetime with the surface temperature for distilled water. . . . .	52
4.6	Results of the droplet lifetime with the surface temperature for ethanol. . . . .	53

4.7	Results of the droplet lifetime with the surface temperature for iso-octane. . . . .	54
4.8	Results of the droplet lifetime with the surface temperature for n-heptane. . . . .	54
4.9	Results of the droplet lifetime with the surface temperature for mixing 11.1% ethanol and 88.9% n-heptane. . . . .	55
4.10	Results of the droplet lifetime with the surface temperature for mixing 65% ethanol and 35% n-heptane. . . . .	56
4.11	Results of the droplet lifetime with the surface temperature for mixing 90% ethanol and 10% n-heptane. . . . .	56
4.12	Results of the droplet lifetime with the surface temperature for gasoline. . . . .	57
4.13	Results of the droplet lifetime with the surface temperature for mixing 10% ethanol and 90% gasoline. . . . .	58
4.14	Results of the droplet lifetime with the surface temperature for mixing 20% ethanol and 80% gasoline. . . . .	59
4.15	Results of the droplet lifetime with the surface temperature for mixing 35% ethanol and 65% gasoline. . . . .	60
4.16	Results of the droplet lifetime with the surface temperature for mixing 50% ethanol and 50% gasoline. . . . .	60
4.17	Results of the droplet lifetime with the surface temperature for mixing 65% ethanol and 35% gasoline. . . . .	61
4.18	Results of the droplet lifetime with the surface temperature for mixing 80% ethanol and 20% gasoline. . . . .	62
4.19	Results of the droplet lifetime with the surface temperature for mixing 90% Ethanol and 10% gasoline. . . . .	63
4.20	Nukiyama temperatures for different compositions of ethanol and n-heptane. . .	64
4.21	Nukiyama temperatures for different compositions of gasoline and ethanol. . .	65
4.22	Frames taken from the test with gasoline on the aluminum surface under film boiling conditions. . . . .	66
4.23	Results of the impact test for n-heptane for different Weber numbers. . . . .	67
4.24	Results of the impact test for n-Heptane with an oxide layer formed on the test section surface for different Weber numbers. . . . .	68
4.25	Outcome of n-heptane droplet impacting on a heated copper surface for different Weber numbers. . . . .	68
A.1	Curve calibration for thermocouple 1. . . . .	80
A.2	Curve calibration for thermocouple 2. . . . .	80
A.3	Curve calibration for thermocouple 3. . . . .	81
A.4	Curve calibration for thermocouple 1. . . . .	81
A.5	Curve calibration for thermocouple 2. . . . .	82
A.6	Curve calibration for thermocouple 3. . . . .	82

C.1	Experimental apparatus used for contact angle measurement (University of Sao Paulo).	85
C.2	Contact angle for single-components on the copper surface (a) and at the aluminum surface (b).	86
E.1	Needle temperature variation with time (test section at 250°C)	89

## List of Tables

2.1	Summary of correlations CHF for prediction (Liang and Mudawar, adapted by author). . . . .	26
2.2	Relationship between wettability and contact angle. . . . .	30
4.1	Fluids used in the tests. . . . .	49
4.2	Values obtained for initial droplet volume, Nukiyama temperature, and Leiden-frost, through experimental tests on pure components and binary mixtures, and predictions of these temperatures by Spiegler <i>et al.</i> (1963) and Habchi (2010) models, and correlations from the Stephan and Abdelsalam (1980), and Ribatski and Jabardo (2003). . . . .	63
B.1	Thermophysical properties of tested fluids (Fardad and Ladommato, 1999, Poling <i>et al.</i> , 2001 and Yaws, 2008) . . . . .	84
B.2	Thermal and physical properties of the wall material used in the tests at 127°C (Misura, 2016). . . . .	84
C.1	Values obtained for contact angle at the copper (cu) and Aluminum (Al) surface. . . . .	85
D.1	Values obtained for droplet impact velocity. . . . .	88

## List of Abbreviations and Acronyms

### *Latin Letters*

$Bo$	-	Bond number	
$c$	-	Specific heat	$[J/(kgK)]$
$D_0$	-	Diameter of the droplet	$[m]$
$f_w$	-	Material parameter in Ribatski and Jabardo correlation	
$g$	-	Acceleration of gravity	$[m/s^2]$
$H$	-	Angle hysteresis	$[deg]$
$h$	-	Heat transfer coefficient	$[W/m^2K]$
$h_{lg}$	-	Heat of vaporization	$[J/kg]$
$k$	-	Thermal conductivity	$[W/mK]$
$L$	-	Heating surface characteristic dimension	
$m$	-	Exponent of $q''$	
$M$	-	Molar weight	$[kg/kmol]$
$Oh$	-	Ohnesorge number	
$P$	-	Pressure	$[Pa]$
$q''$	-	Heat flux	$[W/m^2]$
$r$	-	Multiplication factor	
$Ra$	-	Mean surface roughness	$[\mu m]$
$Re$	-	Reynolds number	
$T$	-	Temperature	$[^\circ C]$
$u_0$	-	Impact velocity	$[m/s]$
$V_0$	-	Initial droplet volume	$[m^3]$
$We$	-	Weber number	

### ***Greek Letters***

$\alpha$	-	Thermal diffusivity	$[m^2/s]$
$\beta$	-	$(k\rho c)^{-1}$	
$\delta$	-	Thickness	$[m]$
$\Delta T$	-	Temperature difference	$[^\circ C]$
$\Delta y$	-	Droplet fall height	$[m]$
$\theta$	-	Contact angle	$[deg]$
$\lambda_v$	-	Thermal conductivity of the vapor	$[W/mK]$
$\mu$	-	Dynamic viscosity	$[Pa.s]$
$\rho$	-	Density	$[kg/m^3]$
$\sigma$	-	Surface tension	$[N/m]$

### ***Acronyms***

CA	-	Contact Angle
CHF	-	Critical Heat Flux
FEM	-	Faculdade de Engenharia Mecânica
MHF	-	Minimum Heat Flux
UNICAMP	-	Universidade Estadual de Campinas

### ***Subscripts***

a	-	Advancing
b	-	Boiling
c	-	Critical
CHF	-	Critical heat Flux
d	-	Departure
f	-	fluid
g	-	Gas
L	-	Leidenfrost
l	-	Liquid
lv	-	Liquid-Vapor
MHF	-	Minimum Heat Flux
N	-	Nukiyama
r	-	Reduced or reduced properties
sat	-	Saturated
sl	-	Solid-Liquid
sv	-	Solid-Vapor
v	-	Vapor
w	-	Wall or apparent

## ***Subscripts***

Y - Young

## ***Other Notations***

$T_L^S$  (°C) - Leidenfrost temperature by Spiegler's model

$T_N^H$  (°C) - Nukiyama temperature by Habchi model

$T_N^{S.A}$  (°C) - Nukiyama temperature through Stephan-Abdelsalam correlation

$T_N^{R.J}$  (°C) - Nukiyama temperature through Ribastsk-Jabardo correlation

# Contents

<b>1 INTRODUCTION</b>	<b>20</b>
1.1 Motivation . . . . .	20
1.2 General objectives . . . . .	21
1.3 Specific objectives . . . . .	21
1.4 Structure of the dissertation . . . . .	21
<b>2 LITERATURE REVIEW</b>	<b>23</b>
2.1 Critical heat flux . . . . .	25
2.2 Leidenfrost effect . . . . .	26
2.3 Correlations and models for single-components . . . . .	27
2.4 Wettability and contact angle . . . . .	29
2.5 Droplet impact on a heated surface . . . . .	32
2.5.1 Droplet impact regimes . . . . .	34
<b>3 MATERIALS AND METHODS</b>	<b>36</b>
3.1 Design and build of the experimental apparatus . . . . .	36
3.2 Experimental setup . . . . .	36
3.2.1 Pneumatic system . . . . .	37
3.2.2 Droplet generation mechanism . . . . .	38
3.2.3 Heating system . . . . .	39
3.3 Test section details . . . . .	39
3.3.1 Data acquisition system . . . . .	40
3.3.2 Recording and lighting system . . . . .	41
3.4 Final arrangement of the experimental apparatus . . . . .	41
3.5 Experimental procedure . . . . .	42
3.5.1 Preparation of the samples . . . . .	44
3.6 Test bench calibration . . . . .	44
3.6.1 Data acquisition system calibration . . . . .	44
3.6.2 Verification test of the droplet volume mean generated by the test needle	47
3.6.3 Thermocouples calibration . . . . .	48
<b>4 RESULTS AND DISCUSSIONS</b>	<b>49</b>
4.1 Results for single-components on copper surface . . . . .	49
Ethanol . . . . .	49
iso-Octane . . . . .	50
n-Heptane . . . . .	51
4.2 Results for single-components on aluminum surface . . . . .	52
Distilled water . . . . .	52

Ethanol . . . . .	53
Iso-Octane . . . . .	53
n-Heptane . . . . .	54
4.3 Results for binary mixtures of ethanol and n-heptane on copper surface . . . . .	55
11.1% Ethanol and 88.9% n-heptane . . . . .	55
65% Ethanol and 35% n-heptane . . . . .	55
90% Ethanol and 10% n-heptane . . . . .	56
4.4 Results for gasoline and binary mixtures of gasoline and ethanol on aluminum surface . . . . .	57
Gasoline . . . . .	57
10% Ethanol and 90% Gasoline . . . . .	58
20% Ethanol and 80% gasoline . . . . .	58
35% Ethanol and 65% gasoline . . . . .	59
50% Ethanol and 50% gasoline . . . . .	60
65% Ethanol and 35% gasoline . . . . .	61
80% Ethanol and 20% gasoline . . . . .	61
90% Ethanol and 10% gasoline . . . . .	62
4.5 Summary of results found through experiments, models and correlations . . . . .	63
Comparison between results obtained for Nukiyama and Leiden-frost temperatures for binary mixtures of Ethanol and n-Heptane . . . . .	64
Comparison between results obtained for Nukiyama and Leiden-frost temperatures for binary mixtures of Gasoline-Ethanol . . . . .	65
Comparison between results obtained for Nukiyama and Leiden-frost temperatures on copper and aluminum surfaces . . . . .	65
Evaporation phenomenon analysis of gasoline on the aluminum surface . . . . .	66
4.6 Weber number influence on the Nukiyama and Leidenfrost temperatures . . . . .	67
<b>5 CONCLUSION</b>	<b>70</b>
5.1 Summary . . . . .	70
5.2 Further work . . . . .	71
<b>References</b>	<b>72</b>
<b>APPENDICES</b>	<b>80</b>
<b>A – Calibration curves and uncertainties analysis</b>	<b>80</b>
A.1 Calibration curve for the copper surface . . . . .	80
A.2 Calibration curve for the aluminum surface . . . . .	81
A.3 Uncertainties analysis . . . . .	82

A.3.1	Test section temperature and digital camera . . . . .	82
<b>B – Properties of test fluids and heating surface</b>		<b>84</b>
B.1	Test fluid properties . . . . .	84
B.2	Heating surface properties . . . . .	84
<b>C – Contact angle</b>		<b>85</b>
<b>D – Impact velocity</b>		<b>87</b>
D.1	Influence of the air resistance force in the droplet . . . . .	87
<b>E – Needle's temperature</b>		<b>89</b>
E.1	Influence of the thermal radiation induced by high temperature of the tests section on the needle's temperature . . . . .	89
<b>F – Pneumatic system code</b>		<b>90</b>

# 1 INTRODUCTION

## 1.1 Motivation

The boiling heat transfer process and the phase change phenomenon during the drop-surface interaction play a significant role in a series of applications and techniques. Generally, the interest in this study is related to refrigeration processes by spraying due to the difficulty obtaining high removal rates heat in confined spaces that comprise electronics packaging, medical equipment, and small devices (Rein, 2002). However, this research topic has been applied in recent years in the automotive area, especially in engines with direct fuel injection in the combustion chamber where the fuel spray can collide with the combustion chamber wall inner. This spray-wall interaction involves different phenomena and depends on the impact conditions (Habchi, 2010). According to Segawa *et al.*, the heat and mass transfer processes inherent to the fuel spray on a heated wall, play an important role in the combustion, ignition, and formation of undesirable pollutants within the combustion chamber. It is important to note that the fuel droplet evaporation on a heated surface is one of the main factors among several processes involved. Besides these applications, this topic also used in the study of systems such as nuclear reactors, power plants, and spray painting (Peyghambarzadeh *et al.*, 2009; Kim, 2015).

The interaction between a liquid droplet and a heated wall is of great relevance when considering several types of boiling phenomena (Someya *et al.*, 2010). Boiling heat transfer is characterized by two key points. The first one is the critical heat flux (CHF) or the Nukiyama point. The CHF represents the operating limit of a system that works under the nucleate boiling regime conditions. In other words, this point represents the maximum capacity these types of equipment in performing its functions efficiently, and therefore, it is considered a design point and one of the main analysis parameters in nucleate boiling processes. This critical point is represented by the Nukiyama temperature ( $T_N$ ) which corresponds to the minimum time of droplet evaporation on a heated surface. An other important feature of the boiling phenomenon is the Leidenfrost point or the intermediate temperature ( $T_L$ ) between the transition boiling regime where the liquid makes direct contact with the solid surface and the film boiling regime when a thin stable vapor layer and is formed between the liquid and the surface during the impact (Nair *et al.*, 2014). The heat transfer rate in the film boiling regime is drastically reduced due to the low thermal conductivity of the vapor layer. This regime should be avoided in applications involving systems that require high heat transfer rates.

The process of the droplet evaporation for single-component liquids has been studied for years, however, experimental data are insufficient for the achievement of the physical patterns during evaporation of droplets composed of mixtures on surfaces with different shapes and orientations (Nakoryakov *et al.*, 2013).

A simple technique used for obtaining such critical temperatures is the droplet evaporation method. This technique requires measuring evaporation times (lifetime) of liquid sessile droplets with a given initial volume over a range of surface temperatures to produce a droplet

evaporation curve (Bernardin and Mudawar, 1999).

## 1.2 General objectives

The objective of this work is based on the droplet evaporation method onto a heated surface to determine Nukiyama and Leidenfrost temperatures for different fluids and mixtures. Compare experimental results obtained through the tests with other experimental data, and values calculated by correlations and models available in the literature, finally, evaluate the influence of the surface material and the Weber number on the Nukiyama and Leidenfrost point.

## 1.3 Specific objectives

- Putting into operation the experimental apparatus;
- Calibrate the experimental apparatus;
- Validate the experimental apparatus
- Measure the total droplet evaporation time (or droplet lifetime) through filming;
- Verify existing correlations in the literature to validate the results obtained through the experiments;
- Identify the Nukiyama and Leidenfrost temperature for each tested fluid;
- To evaluate the influence of Weber number on these critical points.

## 1.4 Structure of the dissertation

In this section, the structure of the present work is briefly described.

In chapter 2 a bibliographical review is carried out, where the fundamental aspects about boiling phenomenon, its regimes, and correlations exist in the literature are presented. Some parameters such as wettability, contact angle, and hydrodynamic aspects in the regime of solid surface droplets are presented in this section.

In section 3 was made a detailed description of the experimental apparatus showing its components. The explanation of the experimental apparatus is divided into subsections for better understanding of the reader. Experimental procedures are detailed throughout the section as well as bench calibration.

The experimental results obtained for evaporation of the droplets tested through the drop evaporation curves as a function of the wall temperature are presented in Chapter 4. Also it is presented a table with the temperature values of Nukiyama and Leidenfrost obtained experimentally together with the temperatures found in the literature, correlations and models.

Finally, chapter 5 presents the main conclusions found in this dissertation and suggestions for future work.

In the appendices are presented the thermocouples calibration curves for copper and alu-

minimum section, experimental uncertainties analysis, and thermophysical properties of the heating surfaces and the tested fluids. The influence of the thermal radiation emitted by the test section on the needle temperature, and, the Arduino code of the pneumatic system is also presented.

## 2 LITERATURE REVIEW

The boiling heat transfer process is characterized by different boiling regimes. Nukiyama (1934) through his experiment that consisted of a electrically heated platinum wire immersed in a reservoir containing water, related the heat flux with wall superheat temperature. This relation was named boiling curve. Figure 2.1 (a) qualitatively depicts the boiling curve (heat flux,  $q''$ , versus the wall superheat,  $\Delta T$ ). Wall superheat is defined as the difference between wall temperature ( $T_W$ ) and the fluid saturation temperature ( $T_{sat}$ ). From the Figure. 2.1 (a), it is possible to identify the main boiling regimes and the same processes are identified on Figure. 2.1 (b).

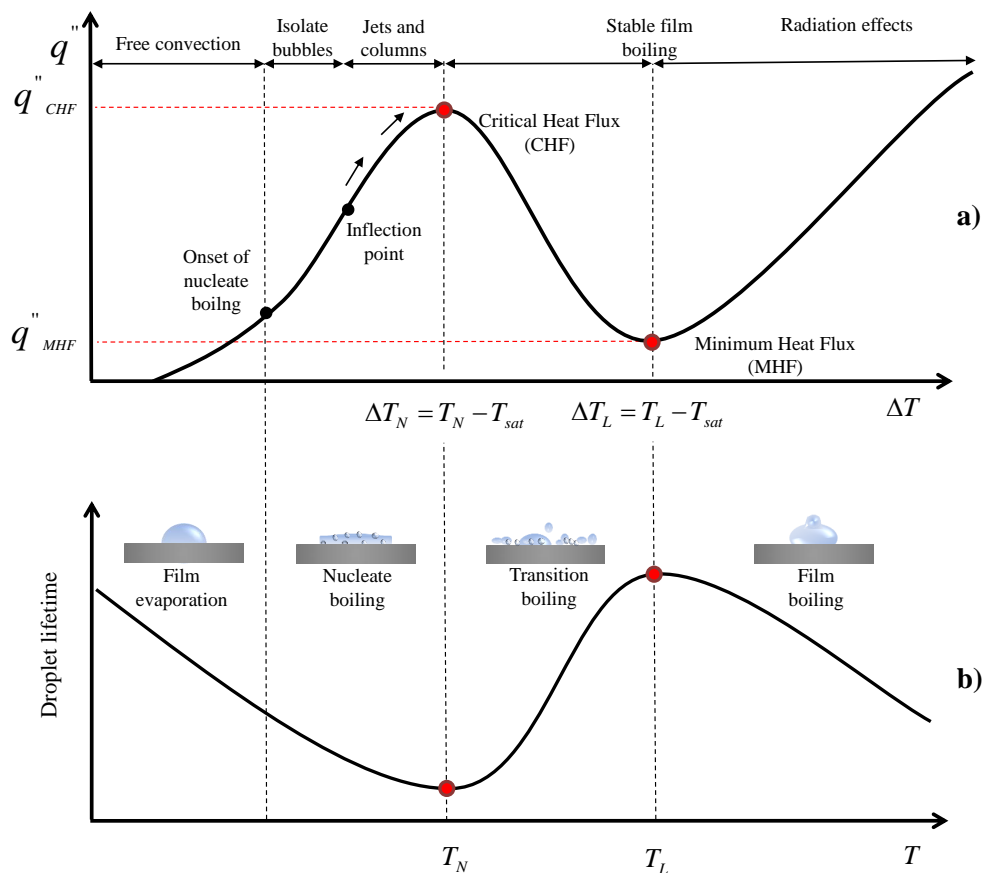


Figure 2.1: Typical boiling (a) and droplet lifetime curve (b) with the critical points.

- **Free convection** ( $T_W < T_{sat}$ ): In this regime the droplet get in contact with the heated wall where  $T_W$  is below the saturation temperature of the fluid, forming a liquid film that evaporates slowly. No bubbles appear and surface heat is removed by convection due to the effects of liquid thrust (Habchi, 2010).
- **Nucleate boiling** ( $T_{sat} < T_W < T_N$ ): Nucleate boiling occurs when wall superheat is sufficient to promote the nucleation of small vapor bubbles that arise through cavities on the surface. These cavities act as nucleation sites which are often the result of roughness found on the heating surface. An increase in heat flux causes the activation of more nucleation sites by increasing the vapor bubble output frequency. This phase change process

does not allow the liquid temperature to exceed its saturation temperature by consuming much of the heat flow transferred to the liquid by the wall (Habchi, 2010). The nucleate boiling regime is characterized by two stages: The first stage comprises a region of low heat flux, called partial nucleate boiling (or isolated bubble region), where discrete vapor bubbles are randomly released by many active sites (Fig. 2.2a). The second stage consists of a region with a high heat flux in which the vapor bubbles agglomerates with other bubbles forming vapor columns (Fig. 2.2b). This region is called fully developed nucleate boiling. At this stage the heat transfer is controlled by a thin layer of adhesive liquid on the heated wall surface.

- **Transition boiling ( $T_N < T_W < T_L$ )**: The transition region is characterized by an intermittent layer of stable vapor on the surface which provides the detachment of large pockets of vapor at virtually identical frequencies. This process can be considered as the initial stage of the subsequent film boiling regime.
- **Film boiling ( $T_W > T_L$ )**: In this regime, due to intense evaporation of the fluid, a vapor layer separates the heated wall from the liquid phase, therefore, the film boiling is not completely dependent on the surface microstructure and the heat transfer process is governed by conduction, convection, and radiation through the vapor layer.

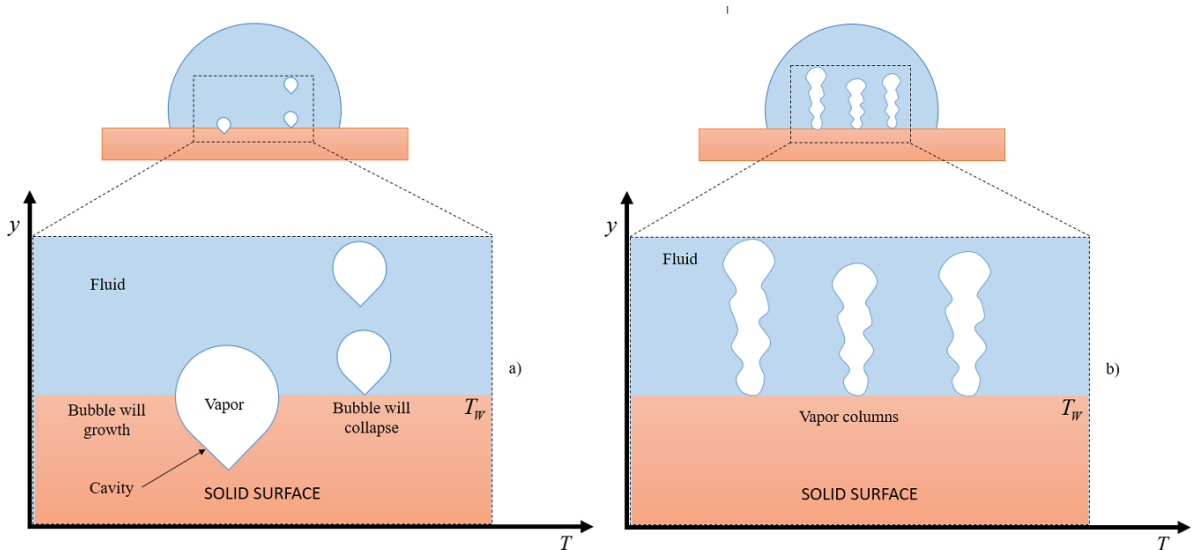


Figure 2.2: Vapor structure in nucleate boiling generated in cavity: discrete bubbles (a), vapor columns (b).

The boiling behavior can also be plotted through Newton's law of cooling (Eq. 2.1) which relates the heat transfer coefficient ( $h$ ) to the wall superheat ( $T_w - T_{sat}$ ). This equation is used in Nukiyama temperature calculations in chapter 4.

$$h = \frac{q''}{T_w - T_{sat}} \quad (2.1)$$

## 2.1 Critical heat flux

Nucleate boiling heat transfer has been studied extensively due to its large industrial application. The performance of the equipment operating under boiling conditions is limited by the transition from the nucleate boiling regime to the film boiling regime. The film boiling region is considered to be an inefficient heat transfer regime being characterized by a dry heating surface, decreasing contact between the liquid and the surface, implied in the reduction of heat transfer coefficient. The phenomenon leading to this transition is called the boiling crisis, and the heat flux at which the maximum performance occurs is CHF (Chu *et al.*, 2013; Theofanous *et al.*, 2002). Therefore, several models have been proposed to explain and predict its occurrence. Theories relating the critical heat flux phenomenon were based on hydrodynamic aspects resulting of the boiling. Kutateladze (1950) was the first researcher to propose a model of boiling crisis. Its model is based on the hypothesis that changes in boiling regimes are the result of the hydrodynamic variation of the two-phases boundary layer, and due to the large turbulence in the viscous boundary layer, both the liquid and the vapor does not influence the process (Yagov, 2014).

Based on the Taylor and Helmholtz instabilities, Zuber (1958) proposed a correlation (Eq. 2.2) taking into account the hydrodynamic instability for an infinite flat plate. He postulates that the vapor generated in the flat plate accumulates in form of continuous column and that the CHF occurs when the liquid-vapor interface of the outlet passage becomes unstable.

$$\ddot{q}_{CHF} = 0.131 \rho_g^{1/2} h_l g [\sigma g (\rho_l - \rho_g)]^{1/4} \quad (2.2)$$

where  $h_l g$  is the vaporization enthalpy,  $\sigma$  is surface tension, and  $\rho_l$  and  $\rho_g$  are the specific mass of the fluid in liquid and gas phase respectively.

Later, Lienhard *et al.* (1973) assumed that the Helmholtz instability is equal to Taylor instability, and suggested the correlation given by the Equation 2.3.

$$\ddot{q}_{CHF} = 0.149 \rho_g^{1/2} h_l g [\sigma g (\rho_l - \rho_g)]^{1/4} \quad (2.3)$$

This model has the following limitations:

- it is for saturated pool boiling only; if the liquid in the pool is subcooled, the critical heat flux is higher;
- It is applicable only to large plates. The characteristic dimension of the plate  $L$  (m) should obey

the Eq. 2.4:

$$L = \frac{32.6}{[g(\rho_l - \rho_g)/\sigma]^{1/2}} \quad (2.4)$$

where  $L$  is given by the shortest side for a rectangular plate or by the diameter for a circular plate. Although the Zuber theory is widely accepted, this model is still quite limited because

disregard the effects of both orientation angle and contact angle.

Liang and Mudawar (2017) collected 18 correlations in their review to predict CHF and classifying them into three groups, the first one being related to the theory of hydrodynamic instability and interfacial lift-off model, the second group taking into account the atmospheric pressure and all orientation angles and finally, the third group takes into account all pressures and orientation angles (see Tab. 2.1).

Table 2.1: Summary of correlations CHF for prediction (Liang and Mudawar, adapted by author).

Authors	Correlations
<i>Horizontal, upward-facing orientation:</i>	
Mudawar <i>et al.</i> (1997)	$\dot{q}_{CHF} = 0.151 \rho_g^{1/2} h_{fg} [\sigma g(\rho_l - \rho_g)]^{1/4}$
<i>Atmospheric pressure, all orientation angles:</i>	
Lienhard and Dhir model modified with Chang and You (1996) Mudawar <i>et al.</i> model modified with Chang and You (1996) Vishnev (1973)	$\dot{q}_{CHF} = 0.149 [1 - 0.0012\theta \tan(0.414\theta) - 0.122 \sin(0.318\theta)] \times \rho h_{fg} \left[ \frac{\sigma g(\rho_l - \rho_g)}{\rho_g^2} \right]^{1/4}$
<i>All pressures and all orientation angles, with contact angles in the range of <math>0 \leq \alpha \leq 90^\circ</math>:</i>	
Kandlikar (2001) Liao <i>et al.</i> (2008)	$\dot{q}_{CHF} = \frac{1+\cos(\alpha)}{16} \left[ \frac{2}{\pi} + \frac{\pi}{4} (1 + \cos \alpha) \cos \theta \right]^{1/2} \times \rho_g h_{fg} [\sigma g(\rho_l - \rho_g)]^{1/4}$ $\dot{q}_{CHF} = 0.131 [-0.73 + [1 + \frac{55-\theta}{100} (0.56 - 0.0013\theta)] \frac{1.73}{1+10-0.0021 \times (1085.4-\theta)}] \times \rho_g h_{fg} [\sigma g(\rho_l - \rho_g)]^{1/4}$

## 2.2 Leidenfrost effect

When a drop is deposited on a superheated solid surface, the exposed liquid in contact with the surface evaporates instantaneously creating a thin vapor layer at the solid/droplet interface (see Fig. 2.3).

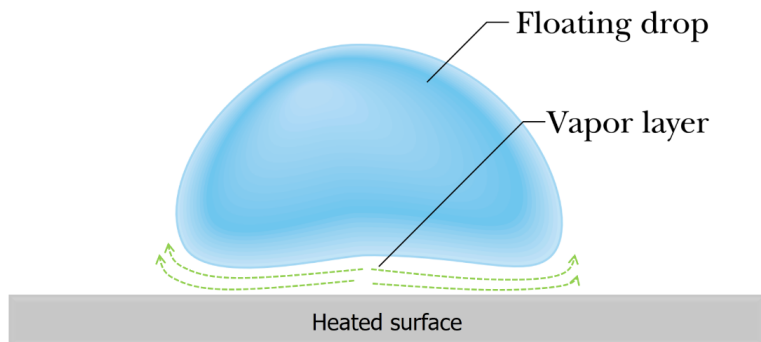


Figure 2.3: Illustration of a droplet in Leidenfrost regime.

The Leidenfrost regime is characterized by a suspended droplet levitating on a vapor layer when the temperature of the heated wall reaches the Leidenfrost point (LFP). The presence of the vapor film between the droplet and the wall surface is a key point from the Leidenfrost phenomenon and may have consequences. One of them is relates the generated vapor ensure a certain degree of thermal insulation, resulting in a droplet evaporation time longer. Another consequence is the minimal friction of the droplet on solid surface, this implies in a greater droplet mobility, enable its manipulation (Talari *et al.*, 2018; Brutin, 2015). According to Talari *et al.* (2018) when the droplet reaches stability under the Leidenfrost regime, the vapor generated at its bottom produces a flow in the radial direction which provides the viscous pressure necessary to suspend the droplet against its weight. The droplet in Leidenfrost point may changes in its shape due to the effect of gravity, where its level of deformation depends on its size (Zhong and Guo, 2017). Rein (2002) explains that small droplets in the film boiling regime assume a nearly spherical shape, whereas larger droplets readily form by gravity. According to Xiong and Yuen (1991), Leidenfrost temperature is independent of the initial droplet volume. However, the same author states that the Leidenfrost temperature is affected by the droplet impact velocity. As this parameter increases, the Leidenfrost temperature increases. For Nakoryakov *et al.* (2012)v also concluded that Leidenfrost temperature is weakly affected by the initial droplet volume. This same author verified that the roughness influences the Leidenfrost point, where its value decreases in polished surface. Segawa *et al.* (2009) found that increasing ambient pressure causes a decrease in Leidenfrost temperature. Already Stanglmaier *et al.* (2002), noted that the droplet lifetime decreases with increasing ambient pressure at the Leidenfrost region.

### 2.3 Correlations and models for single-components

Stephan and Abdelsalam (1980) developed four semi-empirical correlations for estimate the boiling heat transfer coefficient throughn5,000 experimental various data fluids in natural convection boiling heat transfer regime. These researchers used regression methods to develop correlations for water, cryogenic fluids, hydrocarbons, and refrigerants fluids. The Equation 2.5 corresponds to the correlation for hydrocarbons:

$$h = 0.0546 \left( \frac{k_l}{D_b} \right) \left[ \left( \frac{\rho_v}{\rho_l} \right)^{0.5} \left( \frac{qD_b}{k_l T_{sat}} \right) \right]^{0.67} \left( \frac{\rho_l - \rho_v}{\rho_l} \right)^{-4.33} \left( \frac{h_{lv} D_b^2}{\alpha_l^2} \right)^{0.248} \quad (2.5)$$

were bubble diameter  $D_b$  is given by:

$$D_b = 0.0146 \theta \left[ \frac{2\sigma}{g(\rho_l - \rho_v)} \right]^{0.5} \quad (2.6)$$

The authors reported that only some of the 5,000 data found in the literature contained information related to the roughness of the heating surface. In this case, 1  $\mu\text{m}$  was assumed

as value of the average surface roughness. They also affirm that, due to some experimental limitations, it was not possible for the researchers to simultaneously measure the contact angle and the heat transfer coefficient. Therefore, average values for contact angle were utilized for the analyzes. It was assumed for hydrocarbons the value contact angle of  $\theta = 35^\circ$ .

Ribatski and Jabardo (2003) conducted an experimental pool boiling study varying heat flux and reduced pressure across different ranges of average surface roughness for various refrigerant fluids on copper, brass, and stainless steel cylindrical surfaces. Through their experiments, based on 2,600 data for surfaces with a diameter of 19 mm, these researchers proposed an empirical correlation in terms of reduced pressure (Eq. 2.7). The authors compared the data obtained experimentally with the correlations of Cooper (1984), Stephan and Abdelsalam (1980), VDI Heat Atlas modified by Gorenflo *et al.* (1994) and noted that for the surfaces of brass and stainless steel the correlation of modified VDI Heat Transfer compares poorly with experimental data at low reduced pressures, however, an inverse tendency for copper surface was observed.

$$\frac{h}{q''^m} = f_w P_r^{0.45} [-\log(P_r)]^{-0.8} R_a^{0.2} M^{-0.5} \quad (2.7)$$

where  $R_a$ ,  $P_r$ , and  $M$  are: mean surface roughness, reduced pressure, fluid molecular weight respectively, and  $m$  is given by Eq. 2.8.

$$m = 0.9 - 0.3P_r^{0.2} \quad (2.8)$$

Spiegler *et al.* (1963) proposed a model to predict the temperature at which a stable boiling film begins, using as basis the Van der Waals state equation resulting in the represent model:

$$T_L = \frac{27}{32} T_c \quad (2.9)$$

where  $T_L$  corresponds to the maximum liquid superheat (or Leidenfrost temperature) and  $T_c$  is the fluid critical temperature.

The authors affirm that in low pressure conditions (critical below) the equation can generate good results to estimate the wall temperature at the onset of the boiling in stable film. This model showed good accuracy to predict minimum temperatures for cryogenic liquids. In contrast, large errors were observed for water and carbon tetrachloride. It is believed that this discrepancy may be associated with the fact that the Van Der Waals equation does not take into account more complex fluid structures and net surface energy (surface tension). It was observed that fluids with higher surface tension present greater errors in relation to fluids with lower surface tension (Baumeister and Simon, 1973).

Later, Baumeister and Simon (1973) in its work, improved the Spiegler model (Eq. 2.5) through an empirical correlation to determine the minimum temperature of boiling on film, incorporating the physical properties of the heated non-porous surface. However, in this correlation, the authors take no account effect of insulating layer thickness.

$$T_L = T_f + \frac{\frac{27}{32}T_c - T_f}{\exp(0.00175\beta)\operatorname{erfc}(0.042)\sqrt{\beta}} \quad (2.10)$$

where  $T_f$  is fluid temperature (absolute) and  $\beta$  is given by:

$$\beta = (k\rho c)^{-1} \quad (2.11)$$

Habchi (2010), proposed a model to calculate the temperature  $T_N$  corresponds maximum heat flux point, where  $T_b$  is the boiling temperature of the fluid and  $T_L$  is the Leidenfrost temperature.

$$T_N = \frac{T_b + T_L}{2} \quad (2.12)$$

## 2.4 Wettability and contact angle

In recent years, many researchers have reported that surface characteristics as wettability and roughness affect boiling heat transfer phenomenon through the solid-liquid interface (Kim *et al.*, 2016; Li and Huang, 2017). According to Hsu *et al.* (2018), the wettability can vary the temperature at which critical heat flux and Leidenfrost point occurs. Recently, studies have shown that special structure surfaces, like hydrophobic and hydrophilic surface (structures with low and high wettability, respectively), showed enhanced nucleate boiling. (Negeed *et al.*, 2016; Mori and Utaka, 2017; Hsu and Chen, 2012; Jo *et al.*, 2011; Das *et al.*, 2016; Das *et al.*, 2017; Rahman *et al.*, 2014; Dhillon *et al.*, 2015).

The characterization of the wettability phenomenon has shown to be very relevant in industrial processes with applications in the spray quenching and inkjet printing (Seraj and Gadala, 2013 and Fang *et al.*, 2010). Kubiak *et al.* (2011), defined the wettability as the tendency of a liquid deposited on a solid surface under the effect of the gravity spread in this surface until the gravity, capillary, and cohesion forces of the liquid reach an equilibrium state. When the balance between the forces is established, it is possible to measure the contact angle formed in the solid-liquid interface. Marmur (2009) pointed that equilibrium contact angle (CA) is the main property that characterizes wetting systems. The contact angle of the liquid droplet on a solid surface can be defined through the mechanical equilibrium of the droplet under the action of the interfacial tensions or understood as the angle generated between the tangent of the liquid-solid interface and tangent of the liquid-vapor interface (Chau, 2009; Kwok and Neumann, 1999). The interface in which solid, liquid, and vapor co-exist is called of the three-phase contact line (Bracco and Holst, 2013). According to Marmur (2006), the three-phase wetting system (Fig. 2.4) is characterized by three interfacial tensions: liquid–vapor ( $\sigma_{lv}$ ), solid–liquid ( $\sigma_{sl}$ ), and solid–vapor ( $\sigma_{sv}$ ).

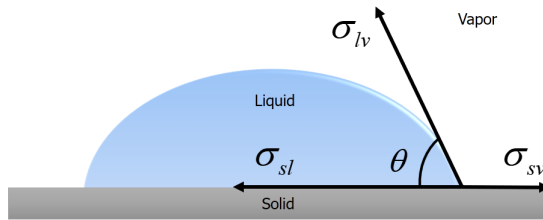


Figure 2.4: Illustrated of system wetting.

The contact angle also indicates the degree of wetting at the moment at which the liquid interacts with a solid surface Fig. (2.5). A surface with a high degree of wettability has contact angle larger than  $90^\circ$  while a surface with low wettability has contact angle values below  $90^\circ$  (Bracco and Holst, 2013). Tab. 2.2 summarizes the relationship between wettability and contact angle.

Table 2.2: Relationship between wettability and contact angle.

Contact angle	Degree of wetting	Strength (solid/Liquid)
$\theta = 0^\circ$	Perfect wetting	Strong
$0^\circ < \theta < 90^\circ$	High wettability	Strong
$90^\circ \leq \theta < 180^\circ$	Low wettability	Weak
$\theta = 180^\circ$	Perfectly non-wetting	Weak

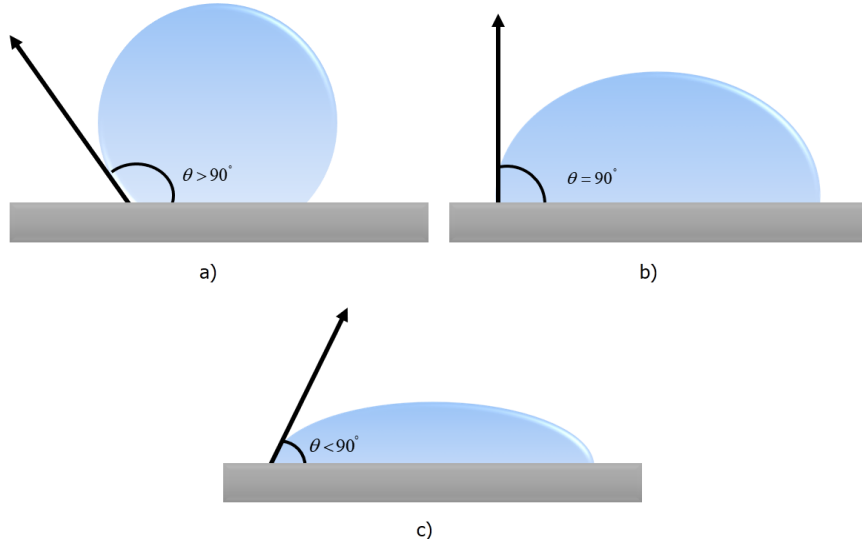


Figure 2.5: Configurations of the solid-droplet interaction with surfaces: no-wetting (a), wetting (b), and totally wetting (c).

Young proposed a theoretical model to estimate the contact angle. He related the surface tension with contact angle in the Equation 2.13 where  $\theta_Y$  is the Young's contact angle.

$$\sigma_{sv} = \sigma_{sl} + \sigma_{lv} \cos \theta_Y \quad (2.13)$$

Young's classical equation is true in conditions of solid surface smooth, flat, homogeneous, inert, insoluble, non-reactive, non-porous (Kubiak *et al.*, 2011; Della Volpe *et al.*, 2002; Gajewski, 2008). The process for reaching steady state is complex, therefore, the Young's angle is an ideal quantity (Della Volpe *et al.*, 2002). Later, Wenzel (1936), proposed a model to calculate the apparent contact angle taking in consideration the effect of surface roughness (Eq. 2.14) where  $\theta_w$  is the apparent contact angle and  $r$  is the ratio of the real rough surface area in relation to the ideal solid surface (Kubiak *et al.*, 2011). For an ideal solid surface, the apparent contact angle is similar to the young's angle due to factor  $r$  assumes the value 1 (Marmur, 2009). Quéré (2008) states that through the Wenzel model it is possible to conclude that roughness enhances wettability on surfaces. In a way that, if the ratio factor  $r$  is greater than 1, a hydrophilic surface becomes more hydrophilic when ( $\theta_w < \theta_Y$ ) while a hydrophobic surface increases its hydrophobicity ( $\theta_w > \theta_Y$ ).

$$\cos\theta_w = r\cos\theta_Y \quad (2.14)$$

According to Chau (2008), the measurement of the apparent contact angle falls into a more or less wide interval between the advancing ( $\theta_a$ ) and receding ( $\theta_r$ ) contact angle (Fig. 2.6), where the difference between these values is denominated the contact angle hysteresis.

$$H = \theta_a - \theta_r \quad (2.15)$$

When the volume of a drop placed on a surface is gradually increased, it may be assumed that the contact line at the solid-liquid interface remains constant while the apparent contact angle is increased until reaching the maximum value (advance angle). If at this point the volume of the drop continues to increase, the contact line promotes the advanced movement. Something similar happens when the volume of the drop is reduced. The contact line remains unchanged at the same time as the apparent contact angle undergoes a process of decrease reaching its minimum limit (recoil angle). If a continuous decreases of the volume extrapolate this limit, the contact line reduced (Fig. 2.6).

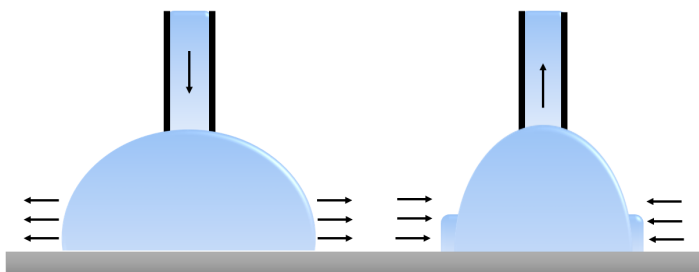


Figure 2.6: Depiction of advancing and receding contact angles.

The contact angle hysteresis is a consequence of the Gibbs energy curve for a non-ideal surface to be characterized by multiple points of minimum or thermodynamically stable appar-

ent contact angles (Fig. 2.7). In this process, the system attempts to achieve a more stable state corresponding to the global minimum energy point. To move from one location to another, the drop must break the energy barrier defined as the energy difference between the minimum and an adjacent local maximum. These movements are known as dynamic wetting (Marmur, 2006). Kubiak *et al.* (2011) reported that hysteresis phenomenon occurs due to characteristics of the surface as roughness and heterogeneity and which the Young's equation became invalid if the roughness is a significant parameter.

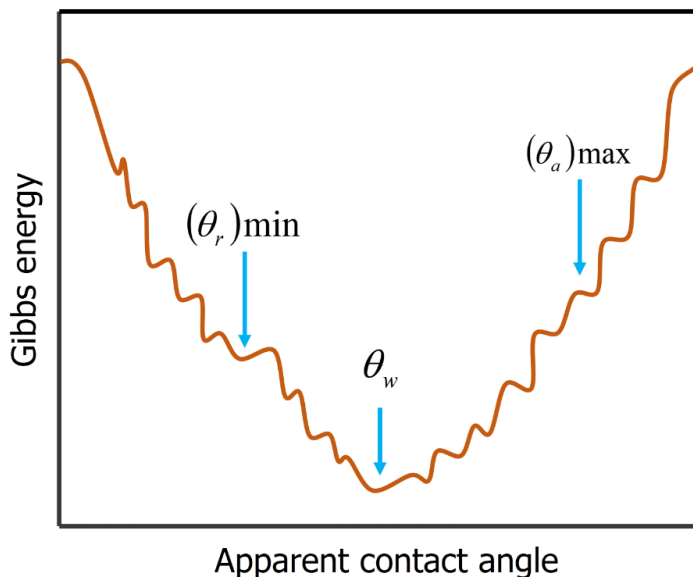


Figure 2.7: Illustrated of the Gibbs energy curve for a real wetting system.

## 2.5 Droplet impact on a heated surface

The boiling phenomenon during the droplet impact on a heated surface occurs on a high surface temperature, implying the nucleation of small vapor bubbles at the solid-liquid interface during droplet spread at the surface, implying the nucleation of small vapor bubbles at the solid-liquid interface during droplet spread at the surface (Khavari *et al.*, 2015). This topic has been pointed out as the basis for explaining in more detail the behavior of the fuel injection systems of internal combustion engines and spray cooling (Moreira *et al.*, 2010; Cossali *et al.*, 2003). Mahulkar *et al.* (2015) in his work mentions that there are appropriate forms for a droplet behavior during the impact on a heated solid surface and these forms depend on the application. According to the authors, in the spray cooling process, it is expected that the total mass to the droplet will remain deposited on the surface, reducing to the maximum its splashing and rebound. However, for fuel injection systems, lower adherence of droplet to the surface is desired, providing a more efficient evaporation process. They also affirm that understanding physical aspects involves interaction between the droplet and a solid surface is essential for handling this interaction. Figure. 2.8 illustrates the main forces acting in the droplet impact process (iner-

tia, surface tension, viscous and adhesion). These forces are governed by numerous parameters such as droplet diameter, impact velocity, including saturation temperature, viscosity, and surface tension relates to the liquid properties influences directly in this process. Characteristics of the solid surface such as diffusivity, wettability, surface roughness and surface temperature are also key parameters in the impact droplet dynamic (Liang and Mudawar, 2017b). Due to this large number variables makes the droplet impact phenomenon become very complex. These variables can be related to dimensionless group such as the Reynolds number ( $R_e$ ), Ohnesorge number ( $O_h$ ), Bond number ( $B_o$ ) and in particular the Weber number ( $W_e$ ) given by,

$$R_e = \frac{\rho_f u_0 D_0}{\mu} \quad (2.16)$$

$$O_h = \frac{\mu}{\sqrt{\rho_f \sigma D_0}} \quad (2.17)$$

$$B_o = \frac{D_0^2 \rho_f g}{\mu} \quad (2.18)$$

$$W_e = (R_e \cdot O_h)^2 = \frac{\rho_f u_0^2 D_0}{\sigma} \quad (2.19)$$

where  $D_0$  is the diameter of the droplet;  $u_0$  is the velocity impact ( $u_0 = \sqrt{2g\Delta y}$ );  $g$  is the gravitational acceleration, and  $\sigma$ ,  $\rho$ , and  $\Delta y$  are, respectively, the surface tension, density of the liquid, and droplet fall height.

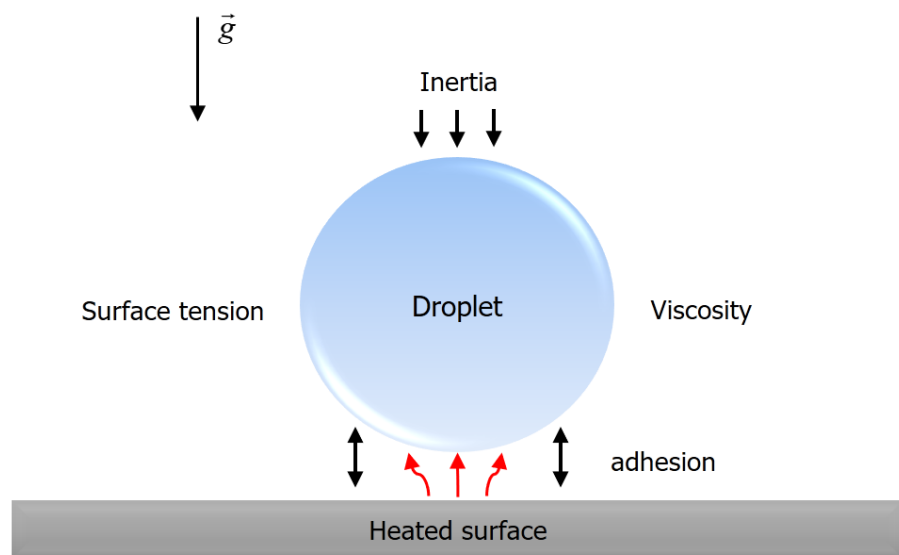


Figure 2.8: Main forces in the droplet impact on a heated surface.

### 2.5.1 Droplet impact regimes

Figure 2.9 shows some possible behaviors of a droplet after its impingement on a solid surface. According to Rein (2002), the droplet impact regime on a solid surface can result in bounced, spreading and splashing. Experiments conducted by Rioboo *et al.* (2001) showed that a droplet exhibits six different behaviors after the collision with a dry solid surface (deposition, prompt surface, corona splashing, receding breakup, partial rebound, and rebound). They reported that after impact, the droplet deposited remaining deformed in the surface. Prompt splashing regime occurs when the liquid spreads in the form of lamella on a solid surface where small drops of the liquid surface can be ejected during this stage. For the corona splashing stage, small droplets are formed away from the solid surface around the corona. For the receding breakup process, after the droplet has reached its maximum spreading, it retracts causing a decrease in the dynamic contact angle and some droplets are left behind by the recessed lamella. For Bertola (2015) the phenomenon of impingement of a drop on a hot surface can be classified in three steps. The first covers period related to the generation of droplet until its impact onto surface. Already the second corresponds spreading droplet that occurs at the moment of impact until its maximum spreading. The author explains that, when a droplet is approximate from a heated surface, it is subject to a counter flux of air. This hot air heats the liquid and reduces the impact velocity of the free droplet. He also states that radiation issued by surface cannot be neglected at high temperatures.

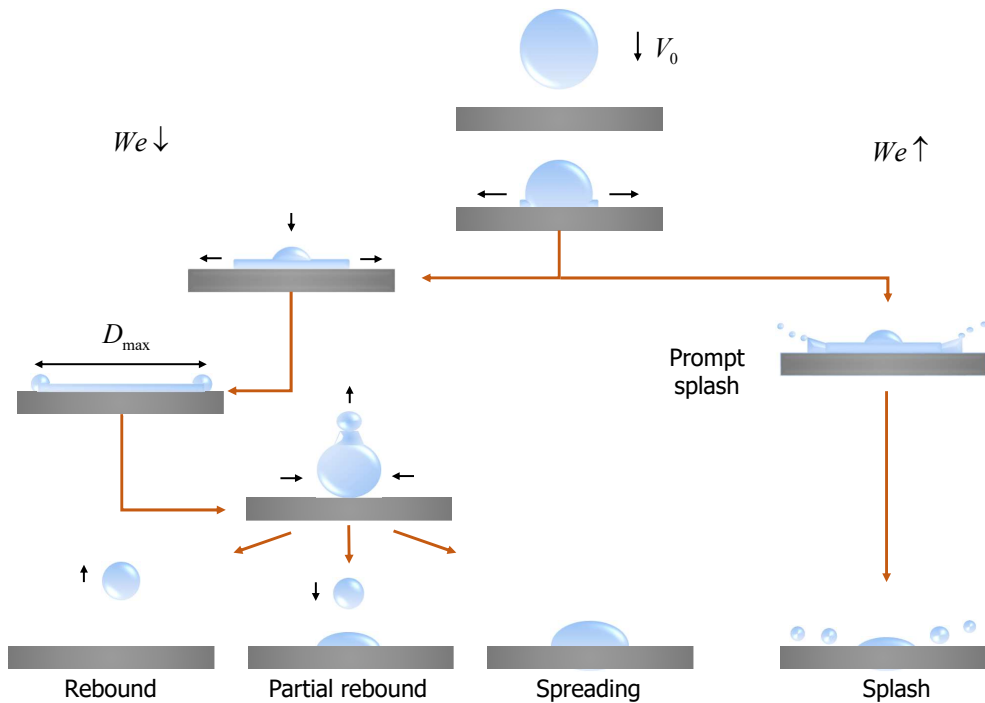


Figure 2.9: Depiction of droplet impact regimes on a solid surface.

According Manzello and Yang (2002), what determines whether a droplet after the impact will spread, splash or rebound, will depend on the impact energy, roughness, and surface temperature. Bertola (2015) explains that the rebound phenomenon at very high surface temperature occurs due to the formation of a vapor film at the interface droplet-wall upon the impact. This vapor layer acts as a kind of lubricant, reducing energy dissipation during the droplet spreading and collecting processes. In this way, there may be a kinetic energetic residue during the retraction process, resulting in the rebound, but the author affirm that if at the end of the expansion there is still excess kinetic energy generated from the impact that has not been dissipated or converted into surface energy, the drop can be fragmented in small droplets. Rein (2002) indicates that the rebound regime is governed by two mechanisms (surface tension and vapor layer at the liquid-solid interface). He reported that during the spread of the droplet in lamella form, surface tension forces act radially towards the center of the lamella, inducing its contraction. The other mechanism is connected to a high pressure gradient in the gap between the droplet and the heated surface. These forces cause a change in the momentum of impact resulting in reflection of the drop. Rein (2002) assert that rebound regime usually occurs at low Weber numbers whereas, for high values of this dimensional number, the partial rebound phenomenon can be observed. Spontaneous droplet spreading is generally driven by surface forces and is retarded by viscous forces (Bayer and Megaridis, 2006). The droplets spread is a consequence of the high pressure imposed after the impaction. The liquid drop extends radially after the impact to relieve this pressure.

### 3 MATERIALS AND METHODS

In this section, the experimental apparatus, calibration method, assembly, and experimental testing are described. The tests were carried out at the University of Campinas, in the Department of Energy, Faculty of Mechanical Engineering, at the Laboratory of Thermal Processes and Environmental Engineering.

#### 3.1 Design and build of the experimental apparatus

To perform this research, it was necessary to design a experimental apparatus (Fig 3.1). The objective is to facilitate and automate the tests, reducing factors that could influence in the experiments repeatability. The test bench was built by the company Magneti Marelli Automotive Systems, Powertrain division and donated to the University of Campinas, School of Mechanical Engineering, where it was carefully instrumented.

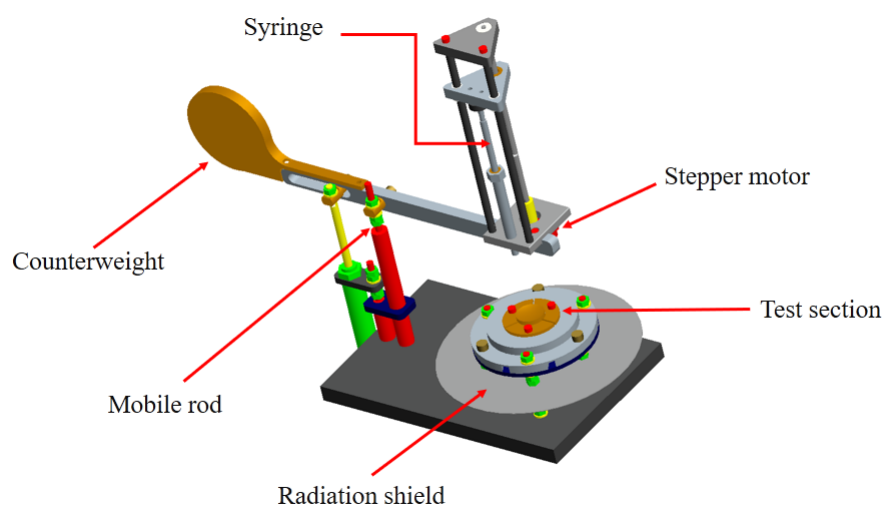


Figure 3.1: Detailed drawing of test bench in CAD.

#### 3.2 Experimental setup

For a better visualization of the experimental apparatus, a schematic drawing was made, showing its main components (Fig. 3.2).

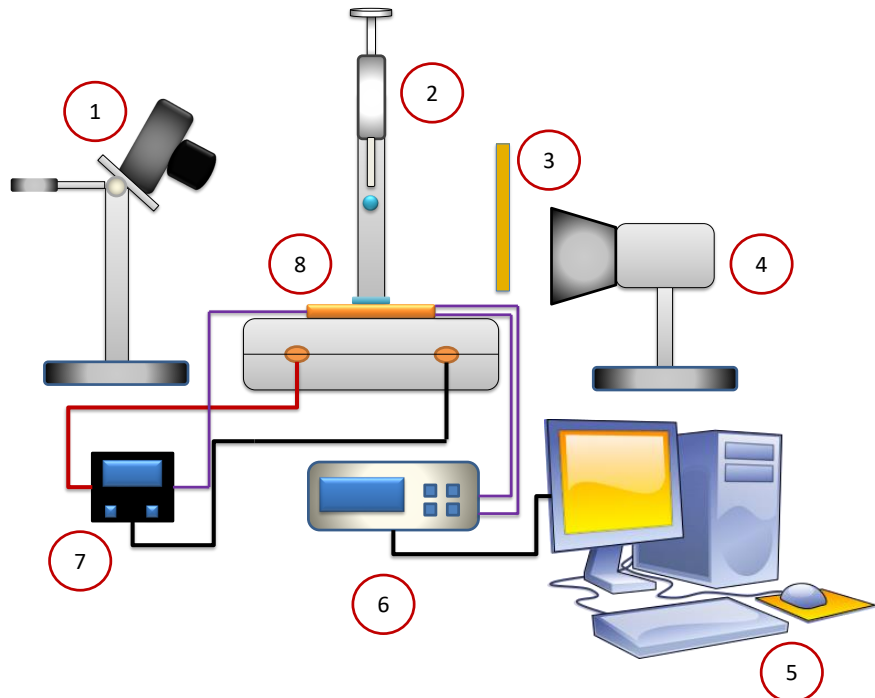


Figure 3.2: Schematic drawing of the droplet evaporation process.

The experimental apparatus comprises the droplet generation section (2) responsible for forming and releasing the droplet, data acquisition system (6), PID controller temperature (7), lighting system and diffuser (3-4), heated test section (8), digital camera (1) and computer (5), dual action pneumatic actuator, pneumatic valve and a power source. For a better understanding, the experimental apparatus was explained in four sections. The first of which comprises the pneumatic part which assists in positioning the syringe relative to the test section; droplet generation mechanism and release; heating system, and data acquisition system.

### 3.2.1 Pneumatic system

The pneumatic system (Fig. 3.3) consists of a pneumatic actuator of double action, pneumatic valve model FESTO, mechanical relay, power source, and system of compressed air. This circuit is activated by a PWM signal generated by an Arduino board and has the purpose of controlling the displacement of the movable rod where the droplet generation mechanism is coupled. When the PWM signal is generated, the pneumatic system request the rod to move downward, positioning the droplet generation mechanism adequately over the test section, after the test has been performed, the rod return to its initial position.

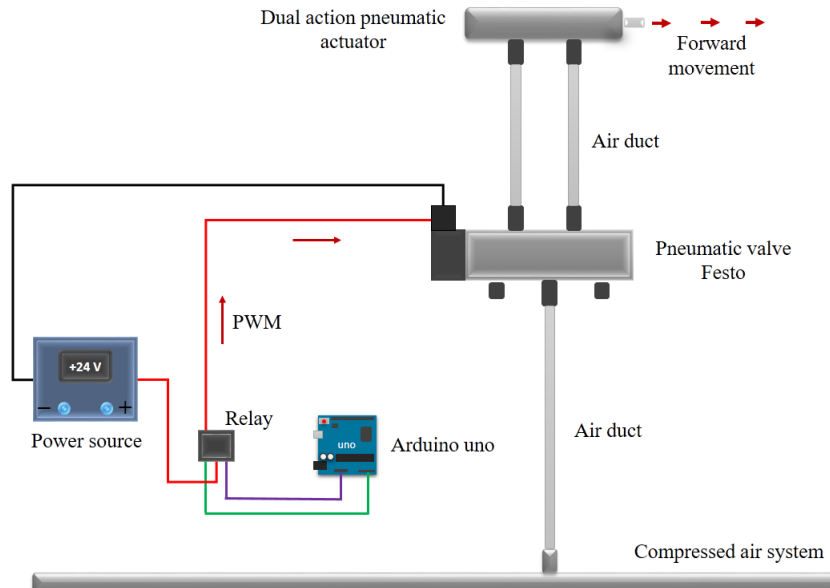


Figure 3.3: Pneumatic system.

### 3.2.2 Droplet generation mechanism

Figure 3.4 shows the main components of the droplet generation mechanism. This section is composed of a stainless steel syringe with capacity of  $2,137 \mu\text{L}$ , a threaded rod, a stepper motor and a movable aluminum plate. The droplet release mechanism controlled by an Arduino board was designed. The plate sends a PWM signal to a stepper motor responsible for turning a threaded rod. This rod makes a rotating movement, causing the moving part of the droplet generation mechanism to move down. In this way, the movable part applies pressure to the plunger of the syringe, generating the droplet.

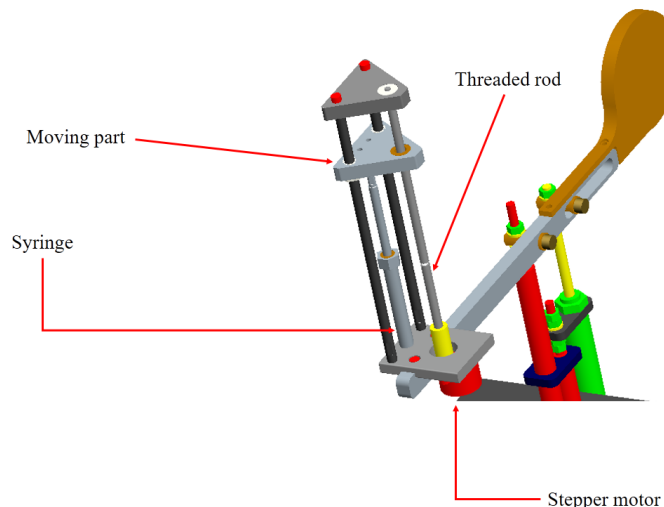


Figure 3.4: Droplet generation mechanism.

### 3.2.3 Heating system

This assembly is responsible for the droplet evaporation process (Fig. 3.5). The heating system consists of an electric resistance, an aluminum block, and a testing section. The aluminum block is divided into two parts, one of which has a channel to attach the resistance and the other part has the role of protecting it and isolating it to prevent its malfunction and risks to the operator.

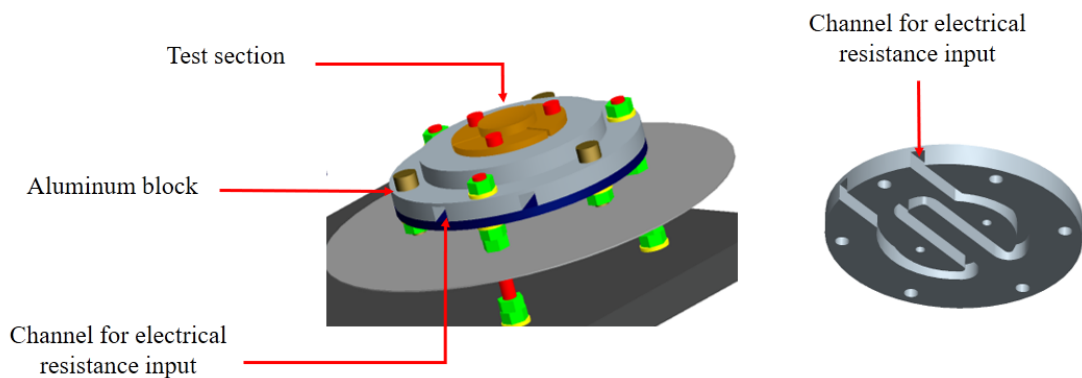


Figure 3.5: Heating system details.

The temperature controller (Fig. 3.6) used to assist the heating system is model 1030 (NOVUS). This device is powered by 100 to 240 vca ( $\pm 10\%$ ), 50/60 Hz, with inputs for type J, K, T and pt100 thermocouples with accuracy of  $\pm 1^\circ\text{C}$ .



Figure 3.6: Temperature controller model 1030 (NOVUS company).

### 3.3 Test section details

The test section consists of a circular copper or aluminum piece with a diameter of 25 mm and a thickness of 7 mm. This piece has three channels for coupling type K thermocouples, where these temperature sensors were soldered at the disk center with tin to ensure a better fixation on the test section. Two of these thermocouples were used to measure the surface temperature through a data acquisition system, while the other is connected to the temperature

controller. The disk has a concave shape to prevent the droplet from leaving the surface during the Leidenfrost regime. A rugosimeter model SJ-210 was used to measure test section roughness. The average roughness value found was approximately  $60 \mu\text{m}$  for copper and  $0.48 \mu\text{m}$  for aluminum respectively.

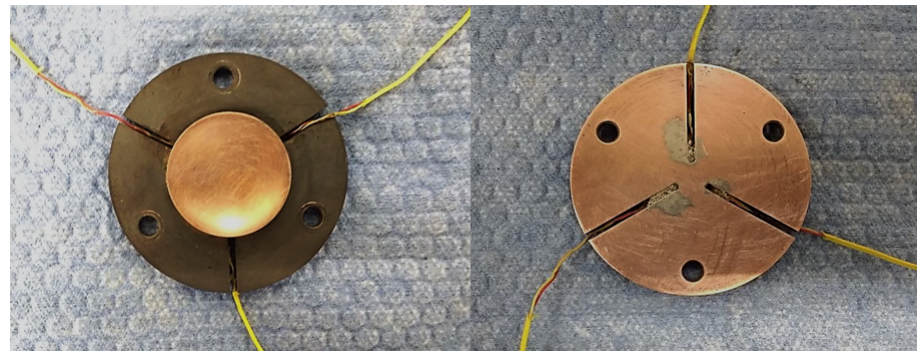


Figure 3.7: Test section with thermocouples.

### 3.3.1 Data acquisition system

The data acquisition system is integrated for a computer-aided reading and acquisition device (Fieldlogger NOVUS model v1.60 as shown in Fig. 3.8) for the configuration and processing of data. The Fieldlogger, has analog, digital, remote, and virtual input channels. The analog inputs are arranged in eight channels for the most diverse types of thermocouples (J, K, T, E, S) and thermoresistances (Pt100, Pt1000). These inputs are configured via software for voltage, current and thermocouple signals. The acquisition equipment can be powered in the range of 90 to 240V, having a 24-bit A/D conversion resolution and its maximum reading rate corresponds to 1000/second. The Fieldlogger is responsible for reading two thermocouples that are connected to the test section, and another thermocouple that register the ambient temperature. Data monitoring is done by software installed on a computer. In order to make data acquisition more accurate during tests, a dry contact switch was installed in the Fieldlogger, enabling the operator to register the temperature of the test disk in the evaporation process.



Figure 3.8: Data acquisition system composed of a computer corporation and Fieldlogger of Novus company (adapted by author).

### 3.3.2 Recording and lighting system

Figure 3.9 shows the recording and lighting system and its key components.

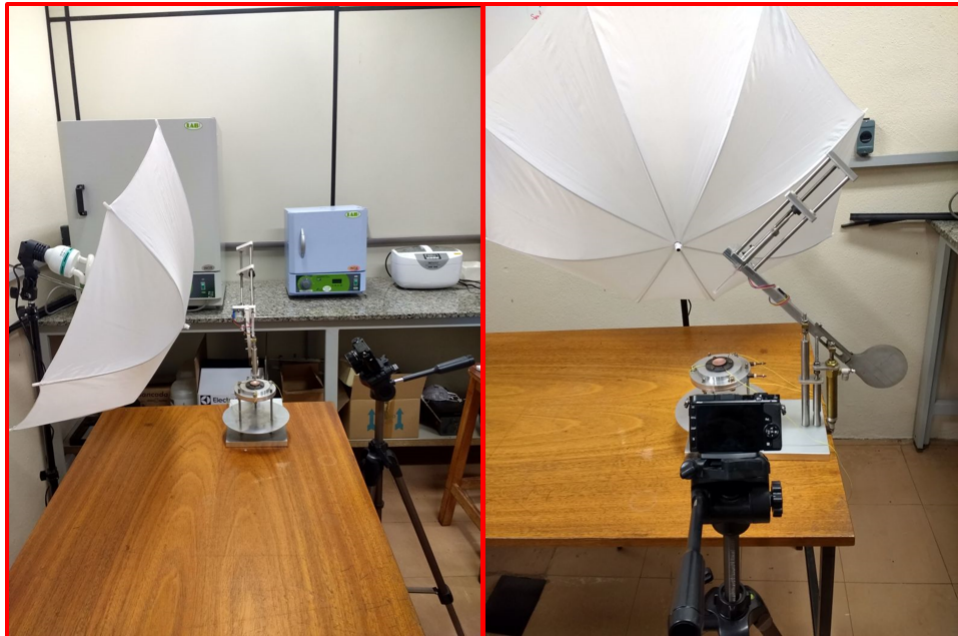


Figure 3.9: Recording and lighting system.

This set consists of a digital camera fixed in an aluminum tripod, a 155 W fluorescent lamp powered by 110V, a white parabolic umbrella diffuser, and a lighting tripod. The model Nikon 1 V3 digital camera CMSO image sensor (Nikon CX format) and 18 million effective pixels. In camcorder mode, it makes HD recordings with a ratio of  $1920 \times 1080 / 60p$  (59.94 frames per second) and slow motion with a ratio of  $1280 \times 720$  (120 frames per second) shot.

### 3.4 Final arrangement of the experimental apparatus

After describing the main components belonging to the test bench, Figure. 3.10 shows the final arrangement of the experimental apparatus in the Laboratory of Thermal Processes and Environmental Engineering.

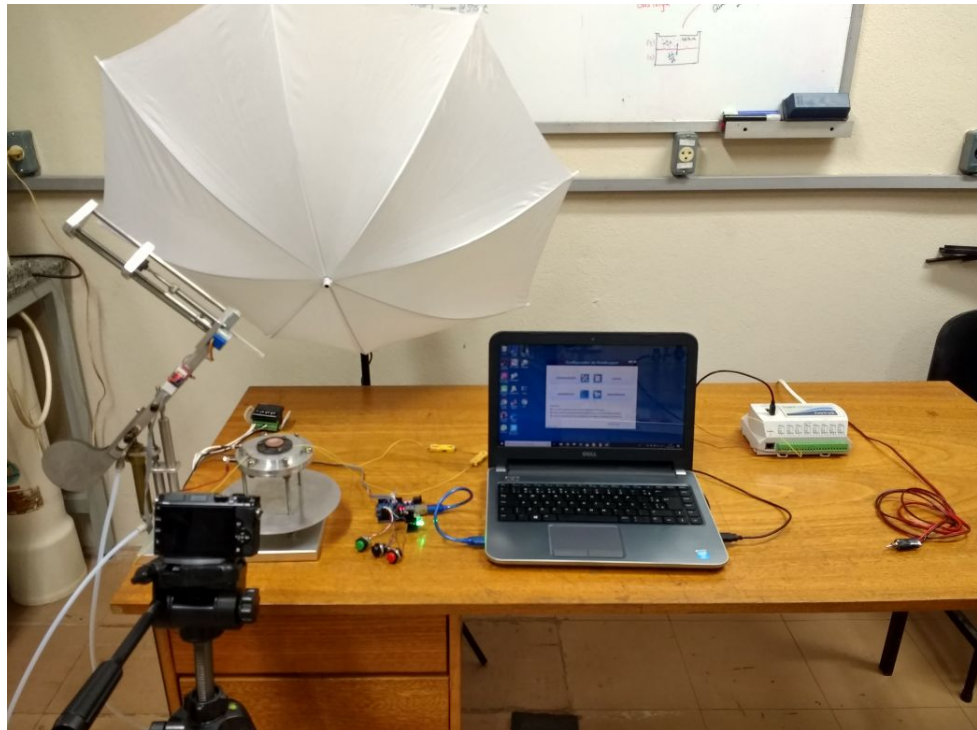


Figure 3.10: Complete apparatus experimental.

### 3.5 Experimental procedure

Before starting the experiments procedure, the test section was carefully sanded in order to remove the oxide layer that forms on the test section surface in high temperatures. The test consisted of dropping a small volume of the test fluid onto a heated surface (temperature higher than the boiling point) and measuring the lifetime (evaporation time) of the droplet (Biance *et al.*, 2003), this method is similar to that described by (Misyura, 2016; Stanglmaier *et al.*, 2002; Fardad and Ladommato, 1999). The procedure is then repeated with various surface temperatures, with droplets of the same approximate volume. The diagram shown in Fig. 3.11, illustrates each step of the test. The stainless steel syringe is fully filled with the test fluid, and placed in the experimental apparatus. The pneumatic system positions the droplet generation mechanism which in turn releases the droplet onto a heated surface. The data acquisition system is activated together with the digital camera that films the entire evaporation process. The captured videos were used to measure the lifetime of the droplet. In this work, the droplets lifetime was estimated from the point where it leaves the needle until it evaporates completely on the surface. It is important to highlight that the experiments were carried out at local pressure and temperature.

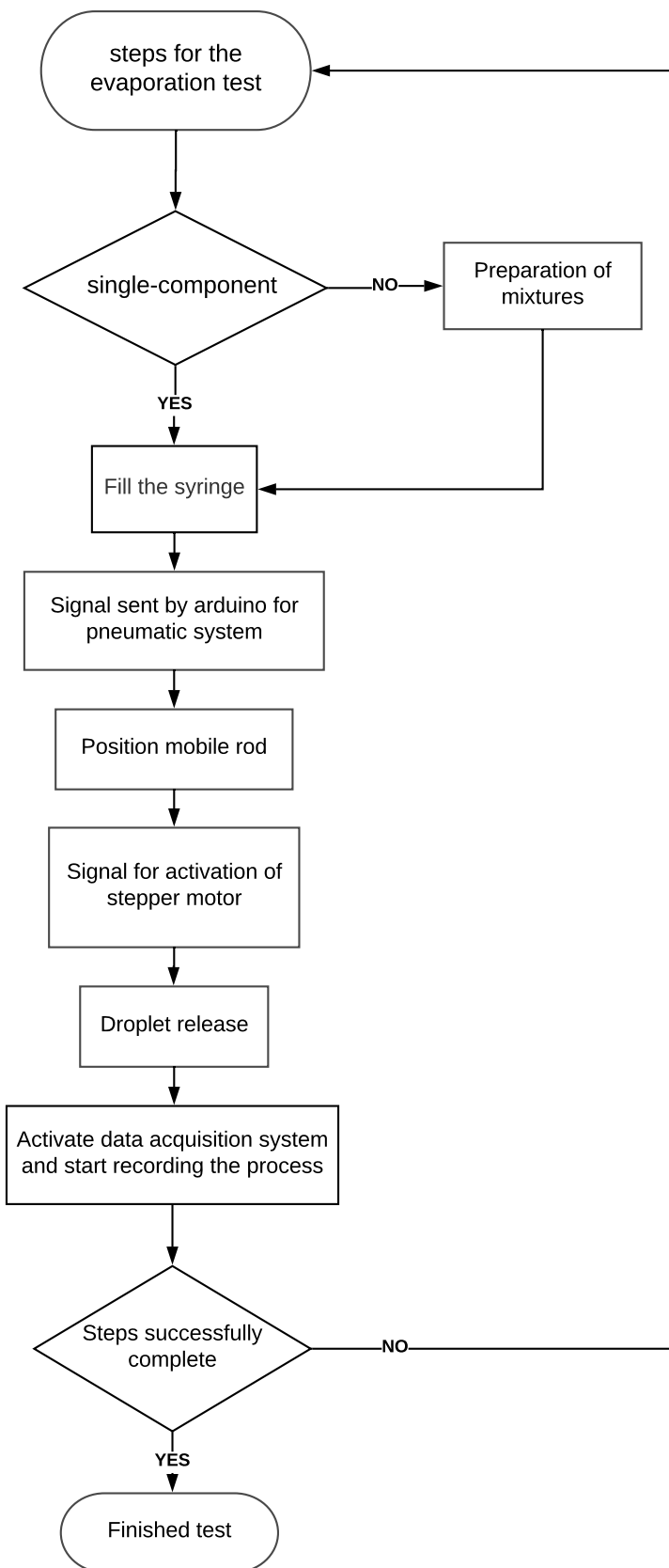


Figure 3.11: Test diagram.

### 3.5.1 Preparation of the samples

To prepare the samples, a graduated glass beaker with a capacity of 200 ml was used, and an analytical balance to weigh the mixtures (see figure 3.12).



Figure 3.12: Items used to prepare the mixtures.

The analytical balance used in this work was OHAUS model PA214CP, with a maximum reading capacity of up to 210 g and a resolution of 0.1 mg. In the case of single-component tests, the fluid is simply placed in the glass beaker (Fig. 3.12) and then sucked through the syringe until it is completely filled. However, for binary mixtures, the process is more complex, requiring the calculation of the percentage of each fluid in molar fraction. The following methodology was adopted: the graduated glass container is placed on the balance where it receives the first component until the balance signals the expected value in mass of the fluid corresponding to the calculated molar fraction. The second component is carefully placed in the beaker until the balance signals the total amount in the mass of the final mixture. The mass value of each component in the mixture was calculated based on the total beaker capacity, addition the desired percentage of each fluid into the mixture.

## 3.6 Test bench calibration

With the objective of guaranteeing a better devices performance which comprises the experimental apparatus, reflecting in more consistent results during the execution of the tests, it was necessary to carry out the calibration of specific equipment such as temperature controller, data acquisition, droplet release system and thermocouples.

### 3.6.1 Data acquisition system calibration

In this step, the input type, its respective unit, and the filter were chosen. Three K-type thermocouple channels were enabled, where two of these sensors record the test section tem-

perature (as mentioned in section 3.3.1). The data collector alarm function has been activated to allows using the dry contact switch, making the timing of data collection more accurate. Once this parameter is enabled, the Fieldlogger can only record data when the switch is triggered. Another important point was to define the data acquisition rate. The criterion for choosing its values took into account the phenomenon speed to be investigated. At the Nukiyama point, the evaporation phenomenon is characterized by occurring in seconds order due to the high heat transfer rates, therefore, the Fieldlogger was configured to obtain high performance with thermocouple scanning rate in 20 ms, and the data acquisition rate set to 100 ms. In contrast, at the Leidenfrost point the values for scan rate and data acquisition were set at 400 ms and 500 ms due to phenomenon occur with higher evaporation time than Nukiyama. The Figure. 3.13, illustrates the scanning and acquisition of data performed by the Fieldlogger.

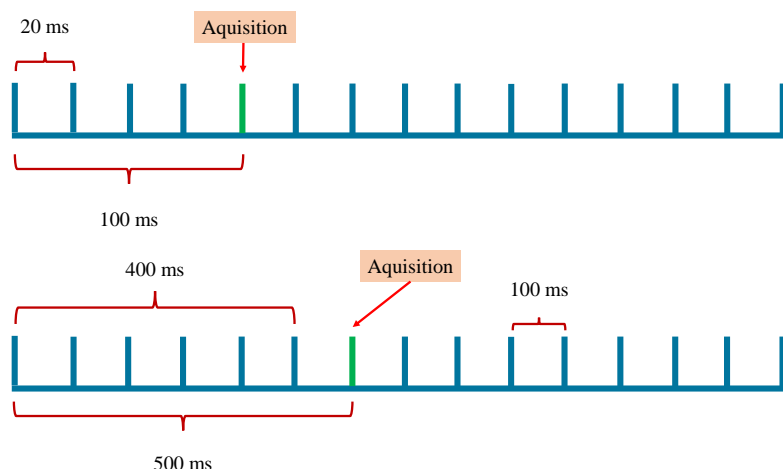


Figure 3.13: Illustrative image of data acquisition dynamics.

Defined scanning values and acquisition parameters, the next step is choosing a data filter (moving average) that is nothing more than the average of the last data acquired. This filter is important due to its function of a data reducing noise. A droplet evaporation test was carried out to evaluate the filter influence on the obtained data in the Fieldlogger. The test consisted of acquiring the droplet's temperature on the test section during the droplet evaporation process distilled water. Eight tests were performed in total, of which four were made with the data acquisition configured with a high acquisition rate, in the nucleate boiling region, and the remainder was performed with a lower acquisition rate in the film boiling region. The test results are shown in the Figures 3.14 to 3.16.

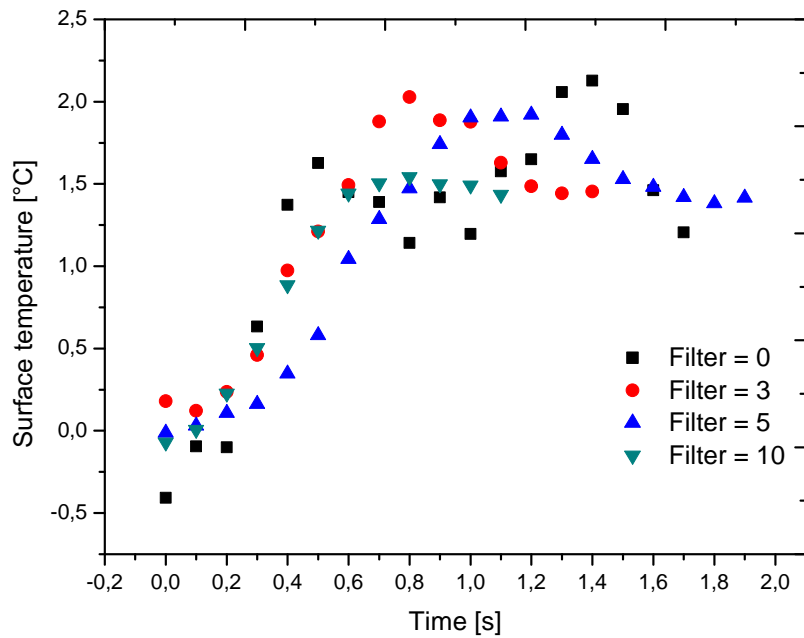


Figure 3.14: Evaporation test of droplet at high acquisition rate with filter value variation ( $T_s = 130^\circ\text{C}$ ).

As can be seen in Figure 3.14, with the increase in the filter value (average), the data recorded by the Fieldlogger is being smoothed due to noise reduction. However, the excessive increase of the filter value, directly affected the results. For the data acquisition close to the Nukiyama point, the filter value of five (average of the last five data acquired) showed to be adequate for performing the tests at a high acquisition rate.

Figure 3.15 shows the result of the evaporation test in the film boiling regime with the configured data acquisition at a low acquisition rate. Through the graph, it is possible to conclude that the filter value five, reduced the noise with a better performance in relation to the other filter values investigated.

For comparison purposes, another test in film boiling regime was performed with the fieldlogger configured at a high acquisition rate and filter set in five (Fig. 3.16). Because the droplet evaporation occurs slowly in this regime, there was a most dispersion of points in the curve, due to a larger number of data collected, making it difficult to visualize the result.

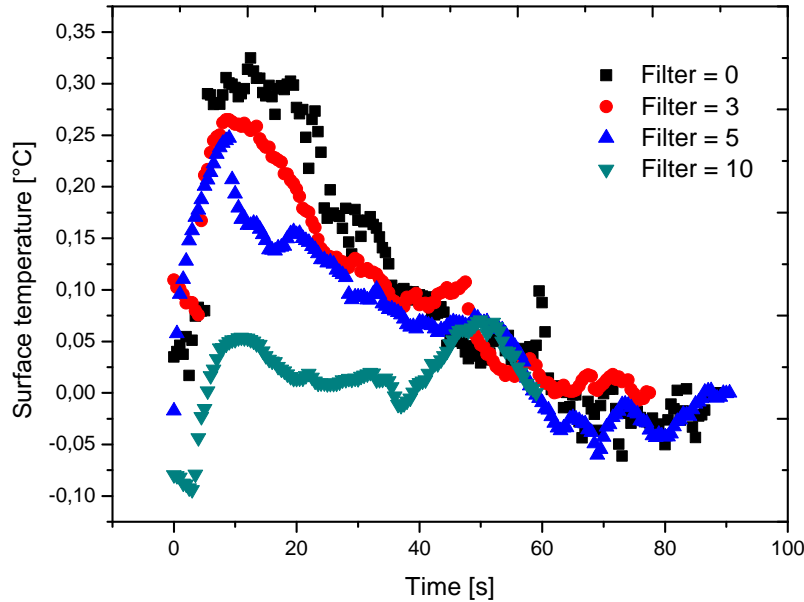


Figure 3.15: Evaporation test of drop at low acquisition rate with filter variation ( $T_s = 230^\circ\text{C}$ ).

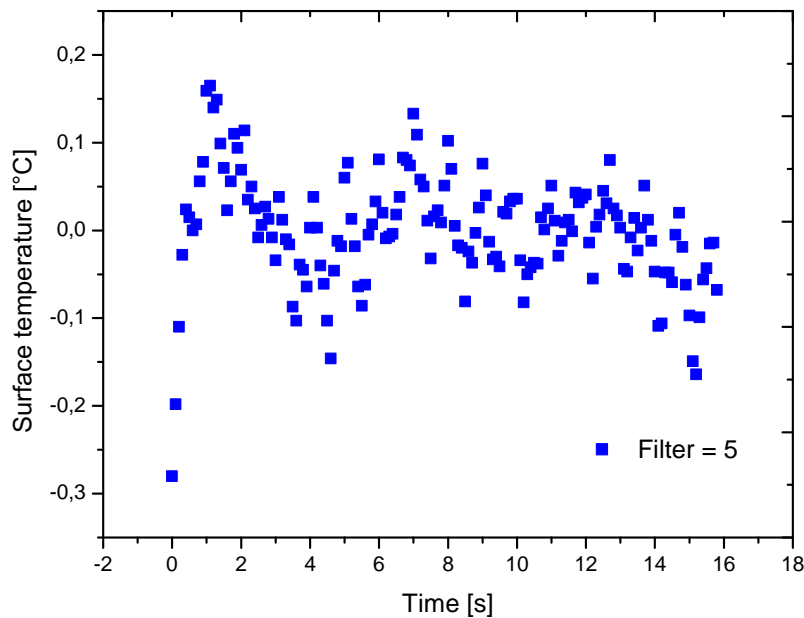


Figure 3.16: Evaporation test of droplet in high acquisition rate in Leidenfrost point ( $T_s = 230^\circ\text{C}$ ).

### 3.6.2 Verification test of the droplet volume mean generated by the test needle

The objective this test was to verify the volume of each droplet generated by the medical needle. The procedure was conducted as follows: initially, the stainless steel syringe was filled with distilled water and carefully fixed to the test bench, where the droplet generation system was suitably positioned on a graduated beaker similar to that of figure 3.12. The test consisted of dripping 50 droplets of distilled water into a glass beaker, and then reading in grams the fluid

amount contained in this receptacle through a precision balance. Each measurement recorded by the balance was converted into volume and divided by the number of droplets generated. This procedure was performed three times and it was found that the volume each droplet generated by the medical needle had a value of approximately  $22 \mu\text{L}$  for distilled water. This method was repeated for each test fluid in order to determine the droplet volume for all.

### 3.6.3 Thermocouples calibration

The thermocouples chosen to be used in the test section were type K, due to their large operating ranges, reaching temperatures up to  $1370^\circ\text{C}$ , and because it has important characteristics such as high thermoelectric power, corrosion resistance and accuracy of  $\pm 0.7^\circ\text{C}$  (Meyer, 1982). The calibration of the temperature sensors was done at the Magneti Marelli Automotive Systems, Powertrain division, which provided the necessary equipment to carry out the work. Three thermocouples were inserted inside a climatic chamber together with a calibrated temperature sensor of the Pt100 type. A data acquisition device was used to monitor and collect the temperatures of each thermocouple at the moment that climatic chamber reaches the desired setpoint and stabilized. The time for this chamber to enter the regime was approximately one hour and a half. During the calibration process, six temperature measurements were collected.

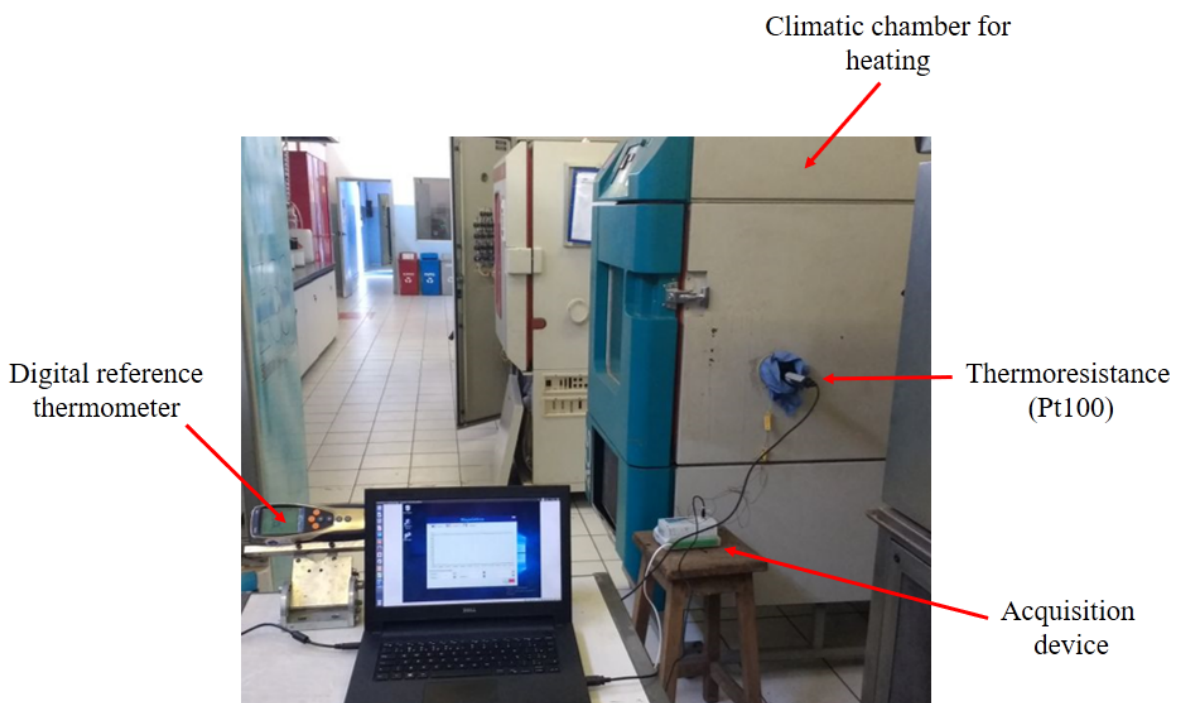


Figure 3.17: Image of the thermocouple calibration process.

## 4 RESULTS AND DISCUSSIONS

This chapter, presented the experimental results obtained during droplet evaporation tests and forward presented all droplets lifetime curves. The single-components and binary mixtures tested are presented in (Tab. 4.1).

Table 4.1: Fluids used in the tests.

Single-components/multicomponent	Binary mixtures
Distilled water	Ethanol / (89.9%) n-Heptane
Gasoline	Ethanol / (35.0%) n-Heptane
Ethanol	Ethanol / (10%) n-Heptane
iso-Octane	Ethanol / (10%) Gasoline
n-Heptane	Ethanol / (20%) Gasoline
—	Ethanol / (35%) Gasoline
—	Ethanol / (50%) Gasoline
—	Ethanol / (65%) Gasoline
—	Ethanol / (80%) Gasoline
—	Ethanol / (90%) Gasoline

Figure 4.1 presents some frames taken from the video used to measure the n-heptane droplet lifetime in a copper surface close to Nukiyama (a) and Leidenfrost (b) temperatures. Through this figure, it is possible to see the fluid different behavior at each point.

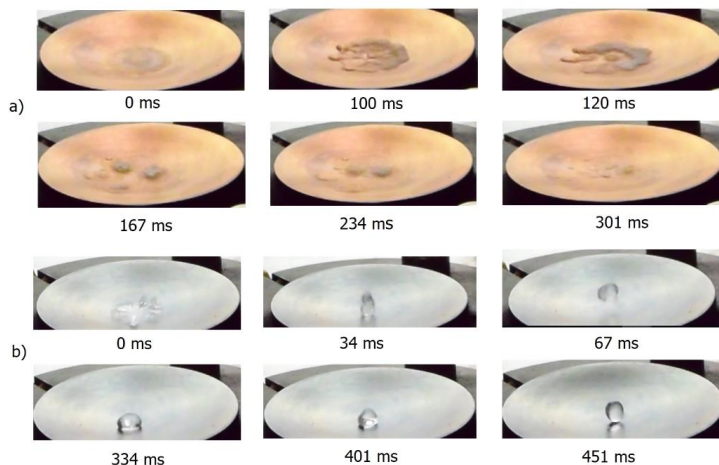


Figure 4.1: Frames taken from the test with n-Heptane: (a) at 125°C; (b) 180°C on the copper surface

### 4.1 Results for single-components on copper surface

#### Ethanol

Figure 4.2 shows the lifetime for evaporation of ethanol droplet with the volume initial of the  $6.88 \mu\text{L}$  on copper surface. The test started at  $70^\circ\text{C}$  where the drop took 16.7 seconds for

total evaporation (region of liquid film evaporation). In the wall temperature between 70°C to 105°C, evaporation of the ethanol droplet gradually decreased. Above 105°C, the evaporation time undergoes a sharp reduction until the Nukiyama temperature is reached. The Nukiyama temperature for this fuel was obtained at  $T_N = 119 \pm 1^\circ\text{C}$  and its minimum evaporation time is approximately 0.18 seconds. Above 130°C the lifetime increased and the process of vaporization of the droplet occurred in a disordered form (transition boiling regime). Large evaporation times began to be observed at wall temperature ranges between 160°C and 220°C. The Leidenfrost temperature was obtained at  $T_L = 200 \pm 3^\circ\text{C}$  with an evaporation time of 26.7 seconds.

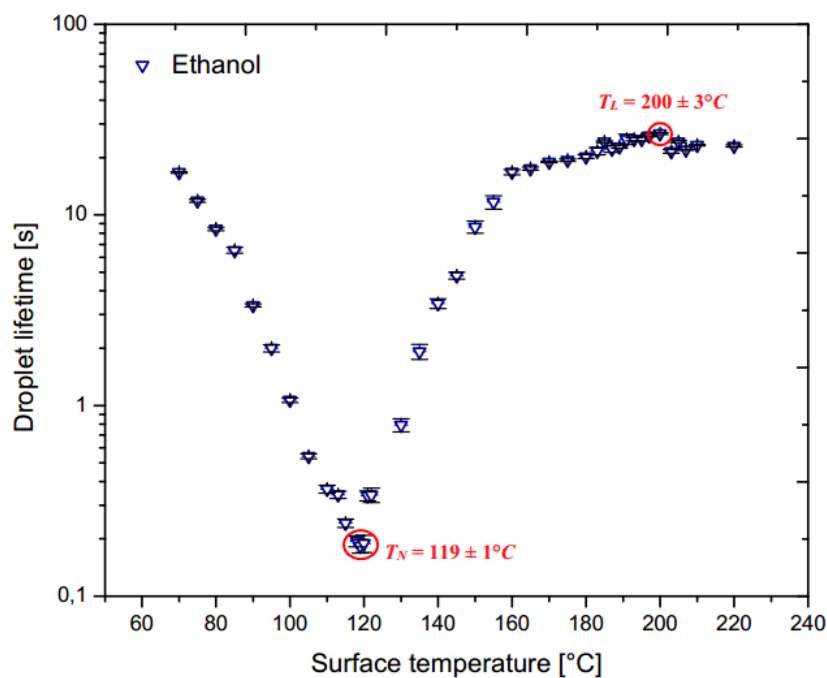


Figure 4.2: Results of the droplet lifetime with the surface temperature for ethanol.

These results show good agreement with the temperatures found by (Oliveira *et al.*, 2015) where  $T_N = 122 \pm 2^\circ\text{C}$  and  $T_L = 190 \pm 5^\circ\text{C}$  and (Habchi, 2010) with  $T_N = 119,25^\circ\text{C}$ . The result obtained for the Leidenfrost temperature is close to the value cited in (Aplinc, 2012), which is around 200°C, but differs with the temperature found by other authors (140°C, 158°C and 160,5°C), by (Mills and Sharrock, 1986; Wang *et al.*, 2000; Spiegler *et al.*, 1963), respectively.

## iso-Octane

For iso-octane (Fig. 4.3), the Nukiyama and Leidenfrost temperatures were determined in  $T_N = 119 \pm 1^\circ\text{C}$  and  $T_L = 175 \pm 5^\circ\text{C}$  respectively. Nukiyama temperature found experimentally differs from the temperature calculated by Eq. (2.12) ( $T_N = 142^\circ\text{C}$ ) but  $T_L$  is close to the temperature caculated by the Spiegler *et al.* (1963) model ( $T_L = 186^\circ\text{C}$ ). Evaporation time at the Nukiyama point for this hydrocarbon differs in relation to ethanol and is around 0.26 seconds, while at Leidenfrost point the evaporation time was approximately 13 seconds.

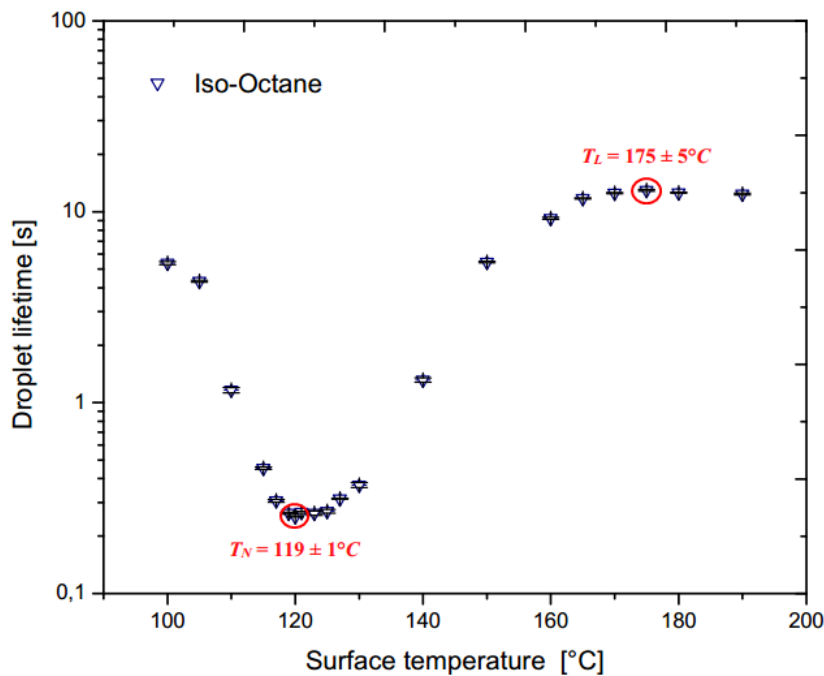


Figure 4.3: Results of the droplet lifetime with the surface temperature for Iso-Octane.

### n-Heptane

Figure 4.4 shows the lifetime for evaporation of n-Heptane droplet with the volume initial of the 7.13  $\mu\text{L}$ .

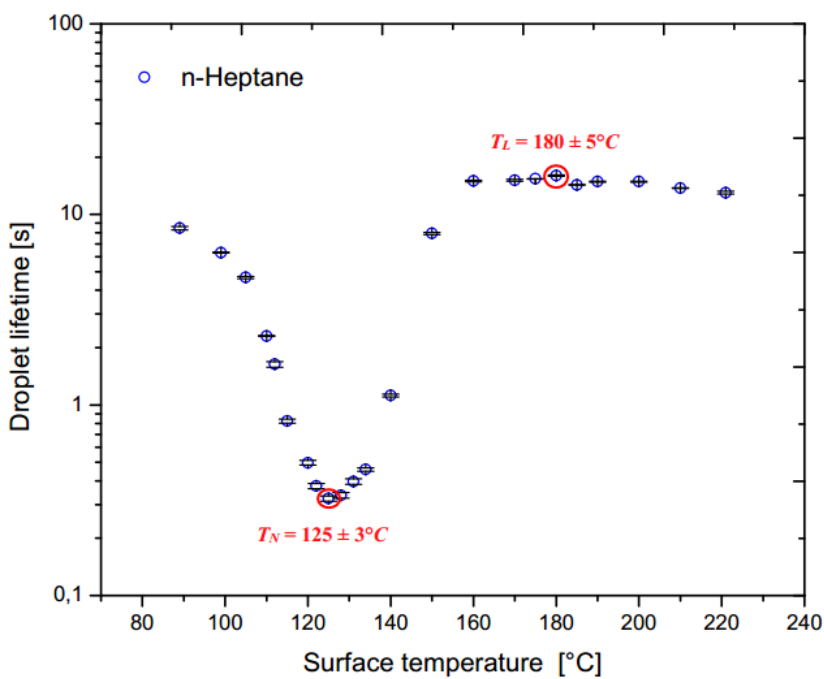


Figure 4.4: Results of the droplet lifetime with the surface temperature for n-Heptane.

The founded Nukiyama temperature for this hydrocarbon corresponds to  $T_N = 125 \pm 3^\circ\text{C}$ , and Leidenfrost temperature corresponds to  $T_L = 180 \pm 5^\circ\text{C}$ . The Leidenfrost temperature found by the Spiegler *et al.* (1963) model ( $T_L = 182.6^\circ\text{C}$ ), is in agreement with the experimental value. The results for n-heptane are close to iso-octane showed above. It is believed that this behavior can be explained because these hydrocarbons have similar physical properties as can be at Appendix. B.2.

## 4.2 Results for single-components on aluminum surface

### Distilled water

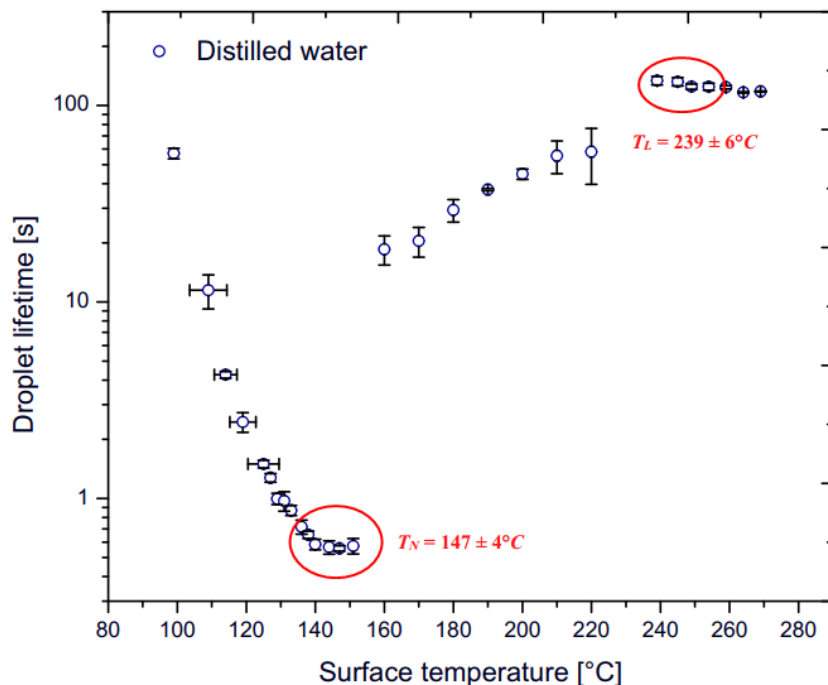


Figure 4.5: Results of the droplet lifetime with the surface temperature for distilled water.

Figure 4.5 shows the droplet lifetime curve of distilled water on Aluminum surface. The nucleate boiling region occurs in a range of 100 to 151°C. From this last temperature, the transition boiling regime begins. It is possible to note the formation of a stable film between the heated surface and the droplet starting at a temperature range of about 233°C. The value of Nukiyama temperature found for distilled water using an aluminum heating surface was around  $T_L = 147 \pm 4^\circ\text{C}$ , while the Leidenfrost point lies within a temperature range of  $T_L = 239 \pm 6^\circ\text{C}$ . The Leidenfrost temperature value is close to the value found by (Baumeister *et al.*, 1970) corresponding to  $T_L = 235^\circ\text{C}$ .

## Ethanol

The droplet lifetime curve of ethanol on aluminum surface is shown in Fig. 4.6. The figure shows that the measured Nukiyama temperature is  $T_N = 108 \pm 3^\circ\text{C}$  with a minimum evaporation time of 0.605 seconds while the evaporation at the Leidenfrost point occurs at a temperature of  $T_L = 160 \pm 5^\circ\text{C}$  and the maximum evaporation time of 48.57 seconds.

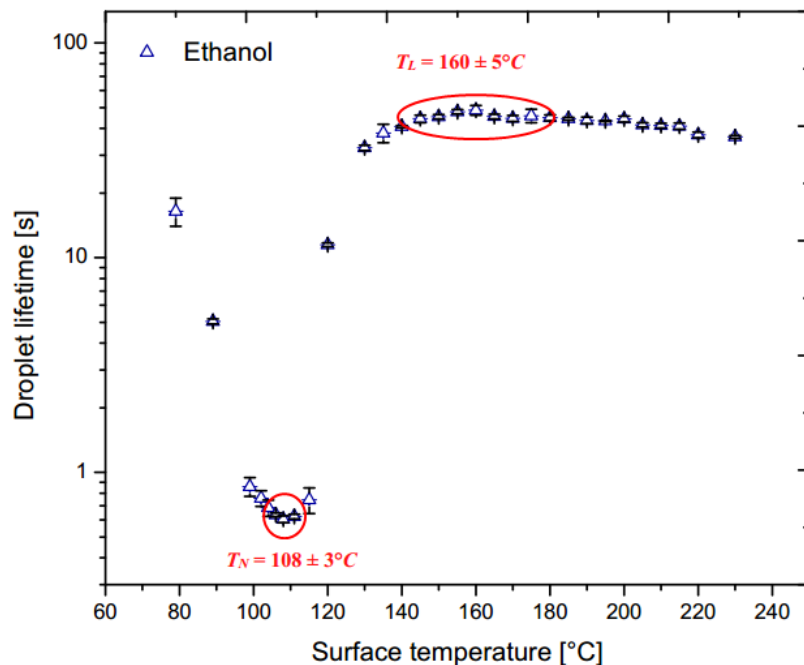


Figure 4.6: Results of the droplet lifetime with the surface temperature for ethanol.

These results show for the Leidenfrost temperature is good agreement with (Spiegler *et al.*, 1963) where  $T_L = 160.5^\circ\text{C}$  and (Baumeister *et al.*, 1970) with  $T_L = 157^\circ\text{C}$ . The Nukiyama temperature for this fluid was not compared with other results due to data limited in the literature.

## Iso-Octane

For iso-octane (Fig. 4.7), the Nukiyama and Leidenfrost temperature were determined in the aluminum surface for  $T_N = 120 \pm 3^\circ\text{C}$  and  $T_L = 180 \pm 15^\circ\text{C}$ . Stanglmaier *et al.* (2002), found these temperatures in the value of 122°C and 190°C for iso-octane using an aluminum surface, while, Baumeister *et al.*, 1970 found the Leidenfrost temperature around 157°C using aluminum as the test section.

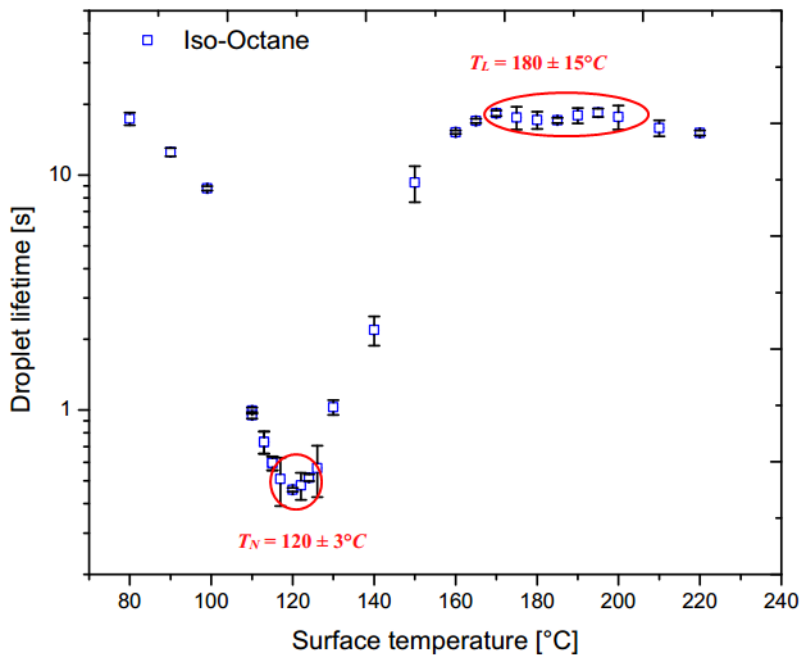


Figure 4.7: Results of the droplet lifetime with the surface temperature for iso-octane.

### n-Heptane

The Nukiyama temperature found for n-heptane on aluminum surface was about  $T_N = 122 \pm 2^\circ C$  while the Leidenfrost point was characterized around  $T_L = 175 \pm 5^\circ C$ . Fardad and Ladommatos (1999), found for n-heptane the Nukiyama temperature around 150°C and Leidenfrost 210°C for a polished aluminum surface.

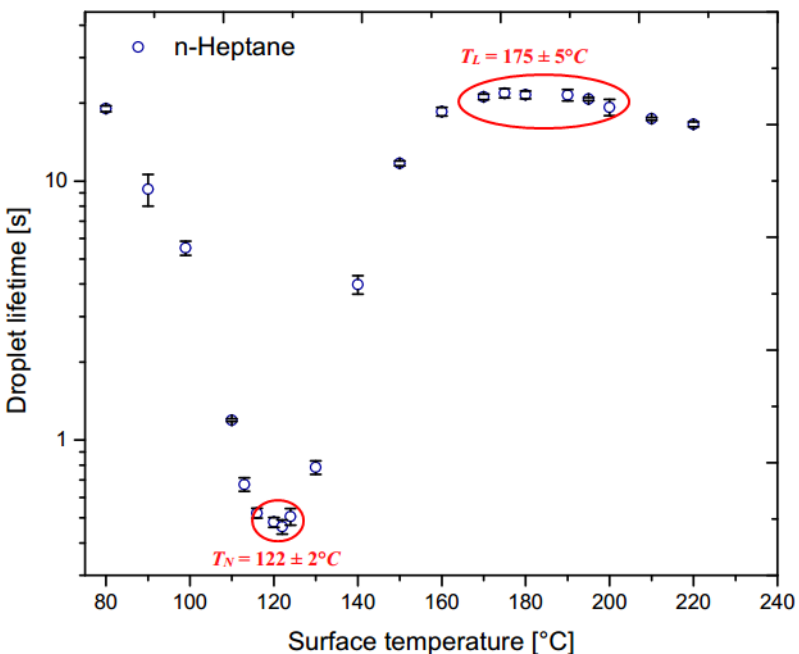


Figure 4.8: Results of the droplet lifetime with the surface temperature for n-heptane.

A similarity is observed in the iso-octane and n-heptane results. One possible explanation would be the fact that these fuels have similar physical-chemical properties(Appendix. B.2).

### 4.3 Results for binary mixtures of ethanol and n-heptane on copper surface

#### 11.1% Ethanol and 88.9% n-heptane

Figure. 4.9 shows the first result founded for a binary mixture. The composition of this mixture was 11.1% Ethanol and 88.9% n-Heptane in terms of the molar fraction. The test was started at 80°C in order to verify how this mixture behaves at the different boiling regimes. For this mixture, the experimental Nukiyama and Leidenfrost temperature observed were,  $T_N = 118 \pm 1^\circ\text{C}$  and  $T_L = 185 \pm 5^\circ\text{C}$  respectively.

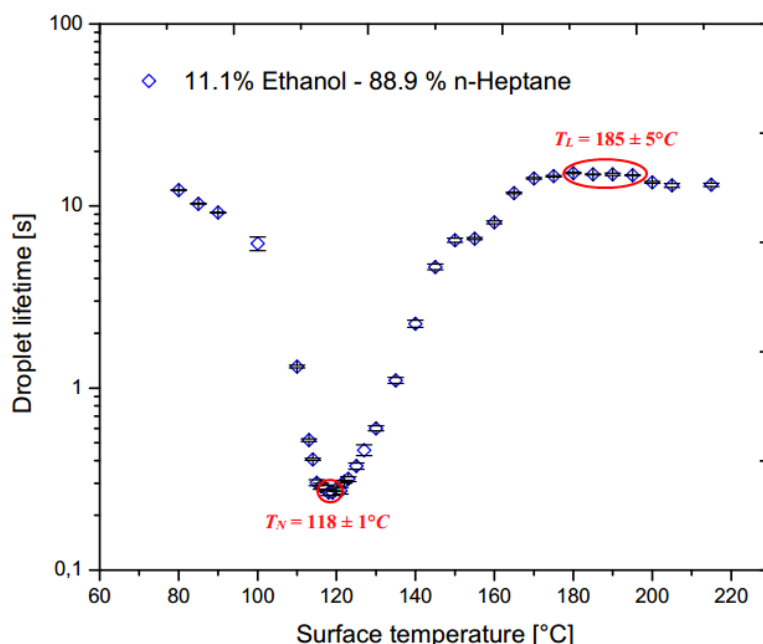


Figure 4.9: Results of the droplet lifetime with the surface temperature for mixing 11.1% ethanol and 88.9% n-heptane.

#### 65% Ethanol and 35% n-heptane

This composition was chosen because it is an azeotropic mixture. The molar fraction of both components are identical in vapor and liquid (for equilibrium), and the bubble and dew point temperatures are similar. Thus, it is expected that exhibit identical behavior to the results presented for single-components. For the present binary mixture, the corresponding value of the Nukiyama and Leidenfrost temperature found were  $T_N = 102 \pm 2^\circ\text{C}$  and  $T_L = 150 \pm 5^\circ\text{C}$  (Fig. 4.10).

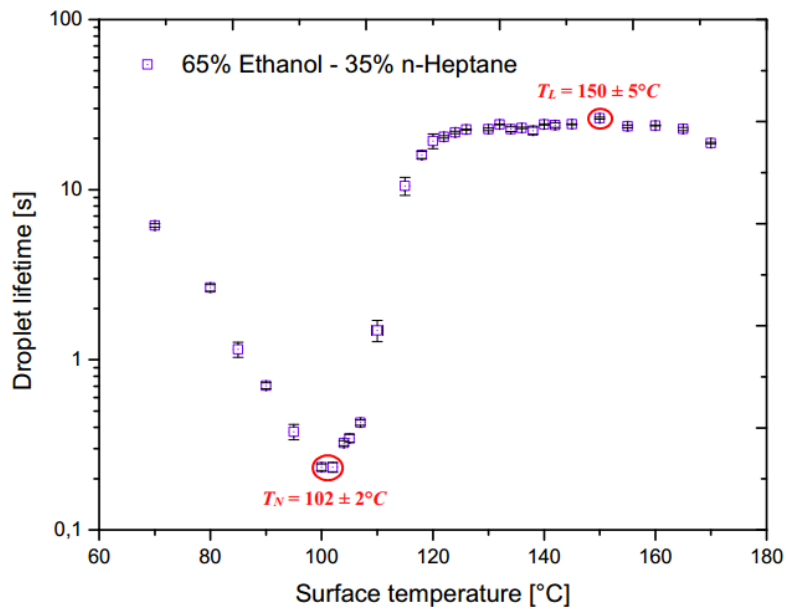


Figure 4.10: Results of the droplet lifetime with the surface temperature for mixing 65% ethanol and 35% n-heptane.

### 90% Ethanol and 10% n-heptane

According to Figure 4.11, for the composition sample corresponding to 90% ethanol and 10% n-Heptane, the found temperature of Nukiyama and Leidenfrost were:  $T_N = 105 \pm 2^\circ\text{C}$  and  $T_L = 195 \pm 2^\circ\text{C}$ .

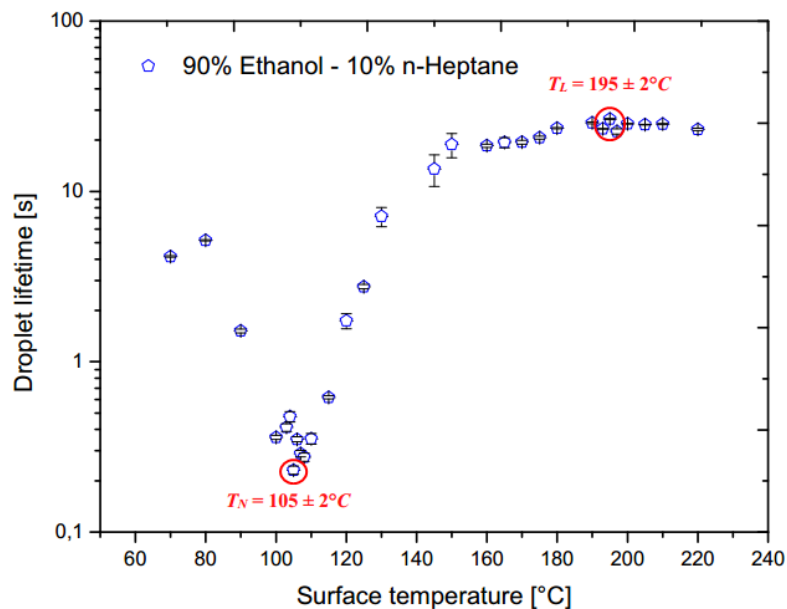


Figure 4.11: Results of the droplet lifetime with the surface temperature for mixing 90% ethanol and 10% n-heptane.

Although this blend has 90% ethanol, the Nukiyama temperature differs considerably

from that found for pure ethanol (Fig. 4.2). However, the Leidenfrost temperature is close to the value found for pure ethanol.

#### 4.4 Results for gasoline and binary mixtures of gasoline and ethanol on aluminum surface

##### Gasoline

Figure 4.12 shows the result of the gasoline evaporation onto aluminum surface. The test was started at a temperature of 120°C covering the entire nucleate boiling region until it reached the minimum point. The gasoline test started with the temperature higher than the other fluids due to gasoline having a great degree of wettability which makes it difficult to visualize the droplet and measure the total droplet evaporation time. At the Nukiyama point the evaporation time was approximately 0.8 seconds. Much longer time compared to other tested fuels. The Nukiyama temperature was characterized by about  $T_N = 180 \pm 2^\circ\text{C}$ . Increasing the temperature beyond Nukiyama point, it is observed that the gasoline evaporates in transition boiling regime, but Leidenfrost temperature for this fuel was not possible to be found due to the droplet evaporate at different times to the same test temperature. This makes it difficult to determine Leidenfrost temperature.

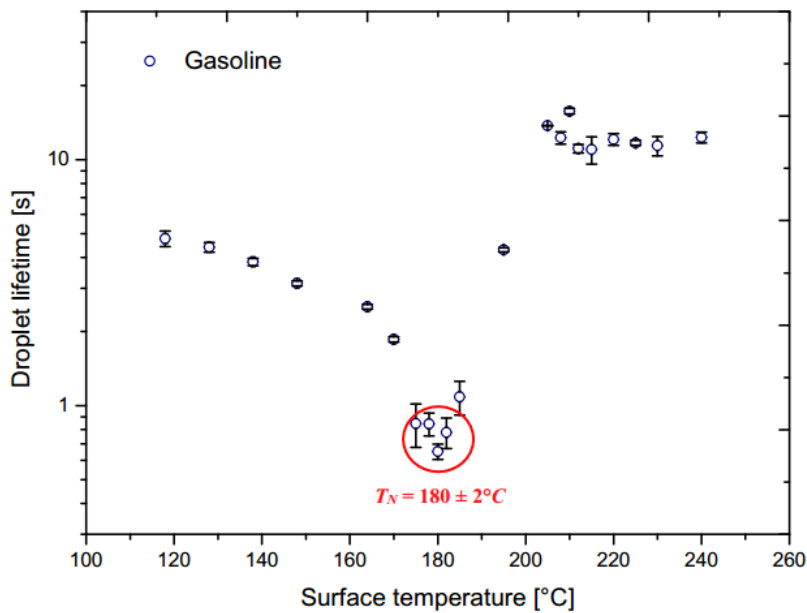


Figure 4.12: Results of the droplet lifetime with the surface temperature for gasoline.

The Nukiyama temperature found in the present work was compared with other works in literature. Fardad and Ladommatos (1999) and Stanglmaier *et al.* (2002), found the Leidenfrost point on the aluminum surface around 180°C for gasoline. The evaporation time corresponding to Nukiyama temperature was close to that found by (Fardad and Ladommatos, 1999) in the

range of 1 second. For the authors cited above, there was a difficulty in determining the Leidenfrost temperature due to large fluctuations in the values of the experimental points in this region.

### 10% Ethanol and 90% Gasoline

Figure 4.13 shows the mixture 10% ethanol and 90% gasoline. The tests started with 160°C due to its high degree wettability which difficult to measure the droplet lifetime. Note that the nucleate boiling regime comprises a temperature range of about 180°C. An increase in the surface temperature beyond that values starts the transition boiling region which extends to a temperature of 200°C initiating the film boiling regime. The found Nukiyama temperature corresponds to  $T_N = 177 \pm 3^\circ\text{C}$ . The Leidenfrost temperature cannot be found due to the experimental points are very close, difficult to characterize this critical point.

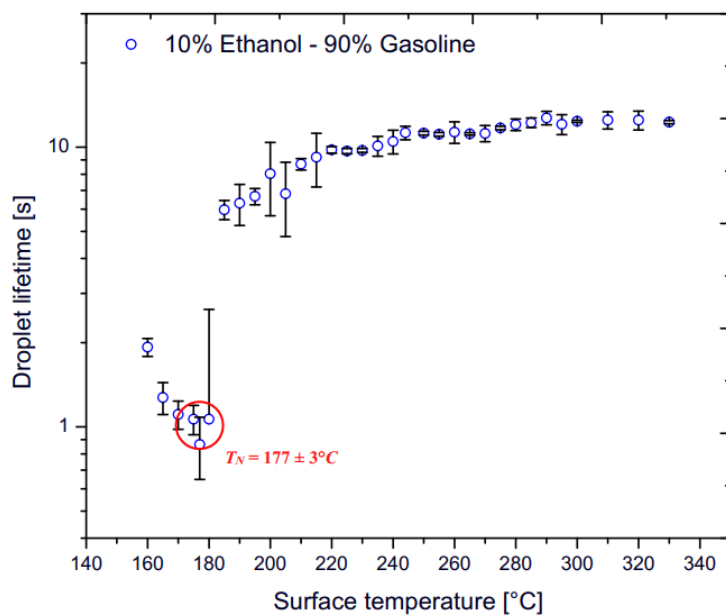


Figure 4.13: Results of the droplet lifetime with the surface temperature for mixing 10% ethanol and 90% gasoline.

### 20% Ethanol and 80% gasoline

Figure 4.14 shows the droplet lifetime result to a mixture of 20% ethanol and 80% gasoline in relation to the surface temperature. The test was started at a surface temperature of 140°C under boiling conditions. The minimum evaporation point was approximately 0.89 seconds and the Nukiyama temperature was characterised at  $T_N = 157 \pm 5^\circ\text{C}$ . The transition boiling regime happened at temperatures between 160 and 200°C giving starting the film boiling regime. For this composition, it was not possible to find the Leidenfrost temperature. It is possible to note that an increase in ethanol composition in the mixture causes a decrease in the Nukiyama tem-

perature.

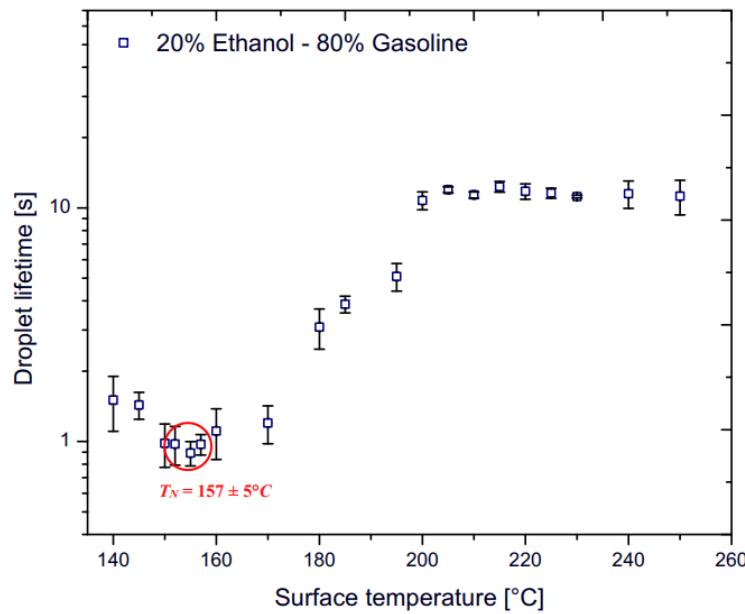


Figure 4.14: Results of the droplet lifetime with the surface temperature for mixing 20% ethanol and 80% gasoline.

### 35% Ethanol and 65% gasoline

Figure 4.15 shows the result for 35% ethanol and 65% gasoline. The test for this composition was started at lower temperatures ( $115^\circ\text{C}$ ) with respect to the compositions shown in the Figures 4.13 and 4.14. The minimum evaporation time was around 1.1 seconds. The Nukiyama temperature was determined at  $145 \pm 5^\circ\text{C}$  and Leidenfrost temperature was obtained at  $T_L = 170 \pm 15^\circ\text{C}$ .

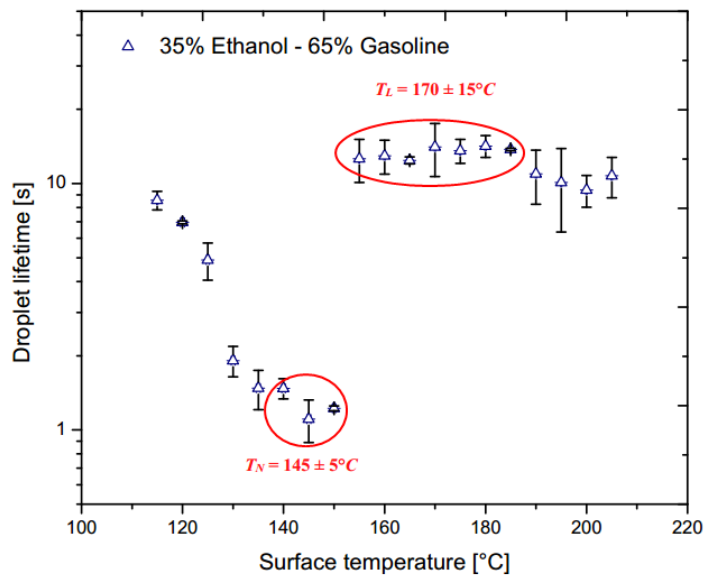


Figure 4.15: Results of the droplet lifetime with the surface temperature for mixing 35% ethanol and 65% gasoline.

It is possible to note a considerable dispersion at the experimental points for this test. This is because of the difference in the droplet evaporation time to a same test section temperature.

### 50% Ethanol and 50% gasoline

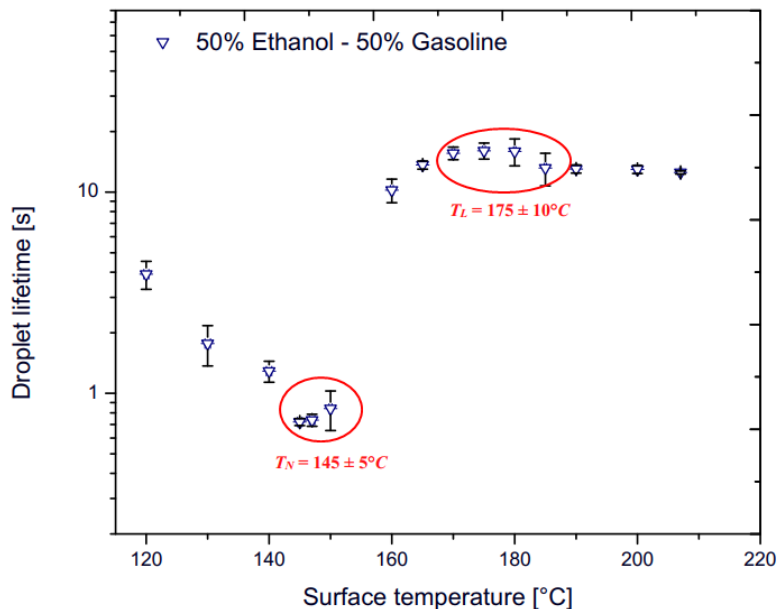


Figure 4.16: Results of the droplet lifetime with the surface temperature for mixing 50% ethanol and 50% gasoline.

The experiment with 50% Ethanol and 50% Gasoline was started at a temperature of 120°C. The nucleate boiling, transition and film boiling regimes are defined as can be observed at Figure. 4.16. It was possible to determine the maximum and minimum evaporation time. For this mixture, the Nukiyama temperature was determined at  $T_N = 145 \pm 5^\circ\text{C}$  with an estimated evaporation time in 0.7 seconds and the Leidenfrost temperature at  $T_L = 175 \pm 10^\circ\text{C}$  with an average evaporation time of 16 seconds.

### 65% Ethanol and 35% gasoline

Through the Figure. 4.17, it is possible to observe the different boiling heat transfer regimes. The test for this sample was started at 120°C (nucleated boiling region). The formation of a stable vapor layer at the solid-liquid interface for this sample started at temperatures close to 160°C. It was possible to determine the Nukiyama temperature around  $T_N = 145 \pm 5^\circ\text{C}$  with the minimum evaporation time of 0.77 seconds. It was not possible to characterize the Leidenfrost temperature with accuracy because the experimental points in the boiling region have a very near evaporation time.

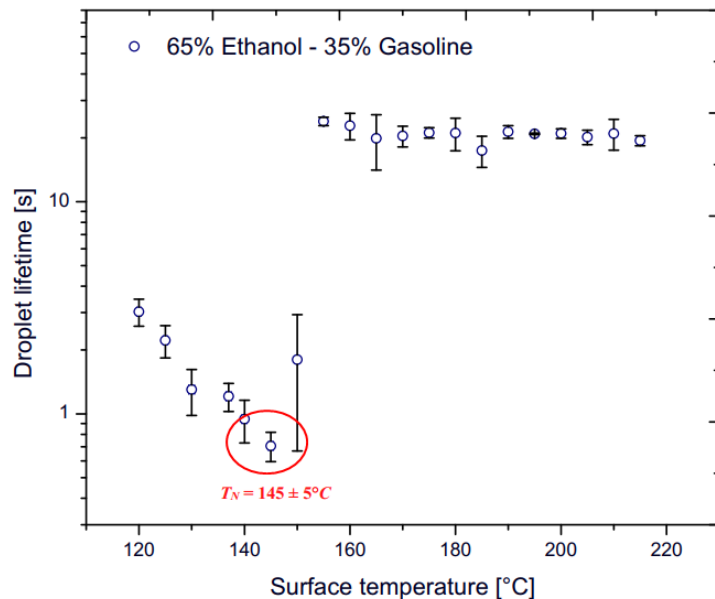


Figure 4.17: Results of the droplet lifetime with the surface temperature for mixing 65% ethanol and 35% gasoline.

### 80% Ethanol and 20% gasoline

The Figure. 4.18 shows the droplet lifetime curve of the 80% ethanol and 20% gasoline.

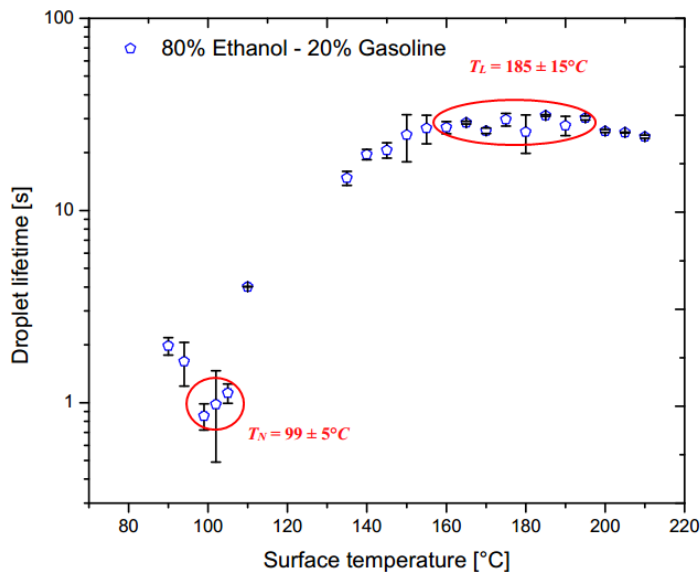


Figure 4.18: Results of the droplet lifetime with the surface temperature for mixing 80% ethanol and 20% gasoline.

For this composition, it was possible to start the tests with lower surface temperatures in relation to the mixtures shown above. This is due to the smaller quantity of gasoline in this mixture. The test covers the nucleate boiling regime until reaching the minimum evaporation time with a value 0.85 seconds where the Nukiyama temperature was found at that point at  $T_N = 99 \pm 5^\circ\text{C}$ . In this figure, it is possible to note that the film boiling regime is better defined in relation to the other results, facilitating the characterization of the Leidenfrost point which had its value characterized at  $T_L = 185 \pm 15^\circ\text{C}$  with an evaporation time of approximately 31 seconds.

### 90% Ethanol and 10% gasoline

The last droplet lifetime curve for gasoline-ethanol blends is shown in the Figure 4.19. For this sample, the test was started with a surface temperature of 85°C. This was possible because this mixture has a smaller quantity of gasoline. The nucleate boiling, transition boiling, and film boiling regimes are well defined in this result. The Nukiyama temperature was identified with value of  $T_N = 104 \pm 2^\circ\text{C}$  with evaporation time of 0.47 seconds, however, the Leidenfrost temperature can not be characterized.

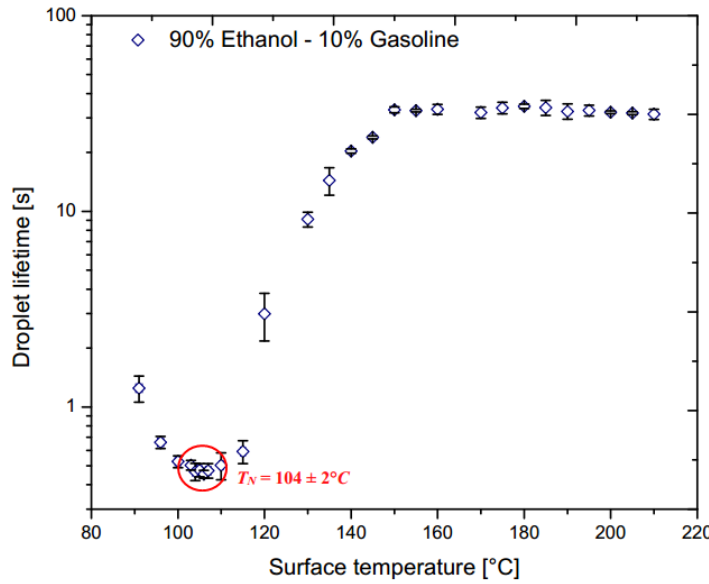


Figure 4.19: Results of the droplet lifetime with the surface temperature for mixing 90% Ethanol and 10% gasoline.

#### 4.5 Summary of results found through experiments, models and correlations

Table 4.2: Values obtained for initial droplet volume, Nukiyama temperature, and Leidenfrost, through experimental tests on pure components and binary mixtures, and predictions of these temperatures by Spiegler *et al.* (1963) and Habchi (2010) models, and correlations from the Stephan and Abdelsalam (1980), and Ribatski and Jabardo (2003).

Fluids	$T_N$ (°C)	$T_N^{S.A}$ (°C)	$T_N^{R.J}$ (°C)	$T_N^H$ (°C)	$T_L$ (°C)	$T_L^S$ (°C)	$V_0$ ( $\mu\text{L}$ )
Distilled Water / Al	$147 \pm 4$	—	—	—	$239 \pm 6$	—	36.8
Ethanol / Cu	$119 \pm 1$	106.1	100.8	119.25	$200 \pm 3$	160.5	6.88
Ethanol / Al	$108 \pm 3$	—	—	—	$160 \pm 5$	—	6.88
Iso-Octane / Cu	$119 \pm 1$	123.24	121.17	142	$175 \pm 5$	186	5.01
Iso-Octane / Al	$120 \pm 3$	—	—	—	$185 \pm 15$	—	5.01
n-Heptane / Cu	$125 \pm 3$	123.8	119.5	140	$180 \pm 5$	182.6	7.13
n-Heptane / Al	$122 \pm 2$	—	—	—	$175 \pm 5$	—	7.13
Gasoline S-50 / Al	$180 \pm 2$	—	—	—	—	—	16.1
Ethanol / (10.0%) n-Hep Cu	$105 \pm 2$	—	—	—	$195 \pm 2$	—	8.43
Ethanol / (35.0%) n-Hep / Cu	$102 \pm 2$	—	—	—	$150 \pm 5$	—	9.02
Ethanol / (89.9%) n-Hep / Cu	$118 \pm 1$	—	—	—	$185 \pm 5$	—	6.53
Ethanol / (10.0%) Gas / Al	$177 \pm 3$	—	—	—	—	—	16.4
Ethanol / (20.0%) Gas / Al	$157 \pm 5$	—	—	—	$185 \pm 15$	—	17.2
Ethanol / (35.0%) Gas / Al	$157 \pm 5$	—	—	—	$170 \pm 15$	—	17.5
Ethanol / (50.0%) Gas / Al	$145 \pm 5$	—	—	—	$175 \pm 10$	—	17.8
Ethanol / (65.0%) Gas / Al	$145 \pm 5$	—	—	—	—	—	18.6
Ethanol / (80.0%) Gas / Al	$99 \pm 5$	—	—	—	—	—	16.9
Ethanol / (90.0%) Gas / Al	$104 \pm 2$	—	—	—	—	—	18.6

In the Table 4.2, the Nukiyama and Leidenfrost temperature on copper (Cu) and aluminum (Al) surface found experimentally are represented by  $T_N$  and  $T_L$ . The results obtained for Nukiyama temperature through Habchi model (Eq. 2.12), and Stephan-Abdelsalam, Ribatski-Jabardo correlations, are indicated by  $T_N^H$ ,  $T_N^{S.A}$ , and  $T_N^{R.J}$  respectively. The values of Leiden-

frost temperature calculated utilizing Spiegler's model are represented in the table by  $T_L^S$ . The Nukiyama temperature was calculated using the equation that relates the heat flux to the heat transfer coefficient (Eq. 2.1).

An important detail and worth mentioning is the fact that all the tests were made with the same needle but the initial droplet volume ( $V_0$ ) of each fuel was different. It is believed that this is a consequence of the property difference for each fluid (Appendix. B.1). The properties necessary to calculate the volume of each droplet was founded at in Poling *et al.* (2001) and Yaws (2008).

### **Comparison between results obtained for Nukiyama and Leidenfrost temperatures for binary mixtures of Ethanol and n-Heptane**

The Figure. 4.20 shows the Nukiyama temperature as according to ethanol composition.

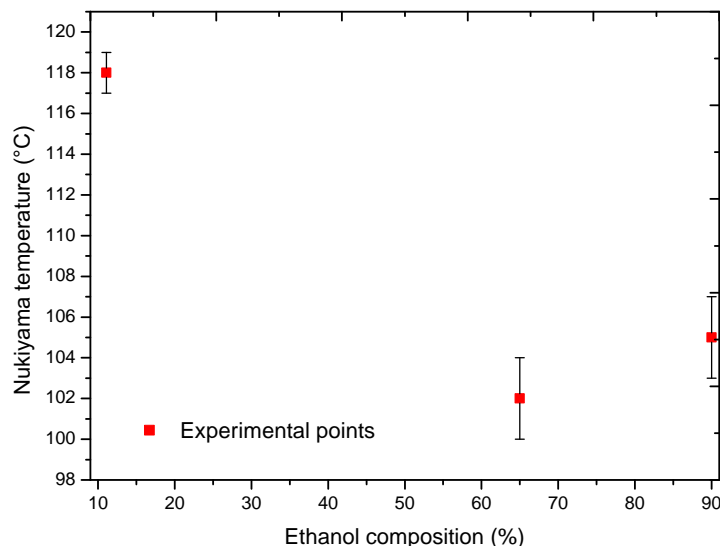


Figure 4.20: Nukiyama temperatures for different compositions of ethanol and n-heptane.

Analyzing the results obtained to ethanol-n-heptane mixtures tests, it is possible to verify that the Nukiyama temperature decreased in the mixtures with a higher ethanol concentration. A possible explanation is that an increase in ethanol concentration can elevate the wettability degree leading to a greater spreading of the test fluid and this may have resulted in a lower Nukiyama temperature. The Leidenfrost temperature underwent a composition decrease with 65% ethanol, however, its value increased in the sample with 90% ethanol. Based on these results it can not be stated that there is a standard for evaporation of these mixtures. Further testing with ethanol and n-heptane mixtures is needed for a more accurate evaluation of the results.

### Comparison between results obtained for Nukiyama and Leidenfrost temperatures for binary mixtures of Gasoline-Ethanol

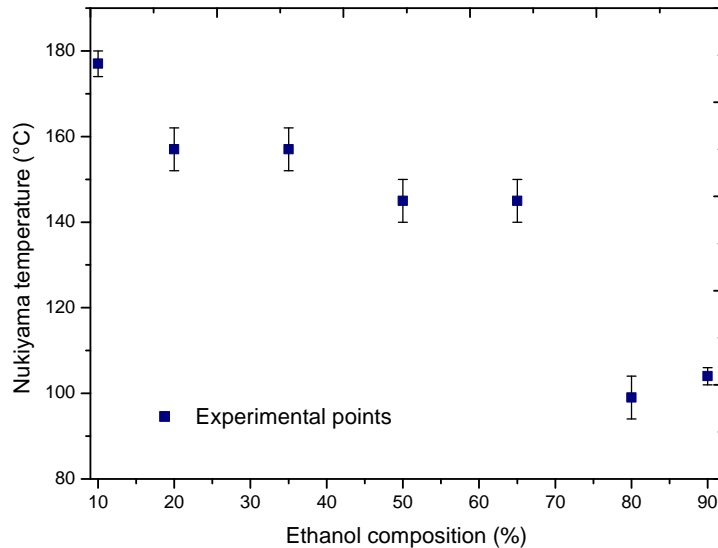


Figure 4.21: Nukiyama temperatures for different compositions of gasoline and ethanol.

According to the data obtained by the tests with gasoline-ethanol blends, it was possible to verify results similar to ethanol and n-heptane mixture (Fig. 4.20). in this specific case, the addition, the addition of the ethanol composition, the Nukiyama temperature had its value reduced (see Fig. 4.21) The same explanation used for mixture and ethanol n-heptane can be applied here. An increase in ethanol concentration can elevate the wettability degree of the mixtures gasoline and ethanol leading to a greater spreading of the test fluid resulting in a lower Nukiyama temperature. At the Leidenfrost temperature, it is extremely difficult to perform an analysis due to the complexity of characterizing this temperature for most samples.

### Comparison between results obtained for Nukiyama and Leidenfrost temperatures on copper and aluminum surfaces

As expected, the heating surface material had some influence on the evaporation of the fuels tested in the present process mainly in the transition region and Leidenfrost point. As can be observed in the Table. 4.2, the Nukiyama temperature with ethanol in the aluminum surface was much smaller the temperature found by using the copper section. In the case of n-heptane, the Nukiyama temperature found in both materials have close values. This was also noted with iso-octane. The Leidenfrost temperature with ethanol in the copper surface has a value higher compared to the results obtained with the aluminum disk. The higher Leidenfrost temperature in the copper section for the ethanol can be explained by the appearance of an oxide layer formed on the surface of the copper during its heating.

For hydrocarbons, the Leidenfrost point for both fluids does not vary much with heating

wall material.

It is also possible to note that the evaporation time for all fluids is higher in the aluminum test section than in the copper section. The heat transfer rate is higher in the copper disk. One possible explanation for these results is the greater roughness present on the copper surface, which may have penetrated through the droplet surface and initiated its internal heating.

### **Evaporation phenomenon analysis of gasoline on the aluminum surface**

The Figure. 4.22 shows same frames of the evaporation process of gasoline on the aluminum surface under film boiling regime conditions.

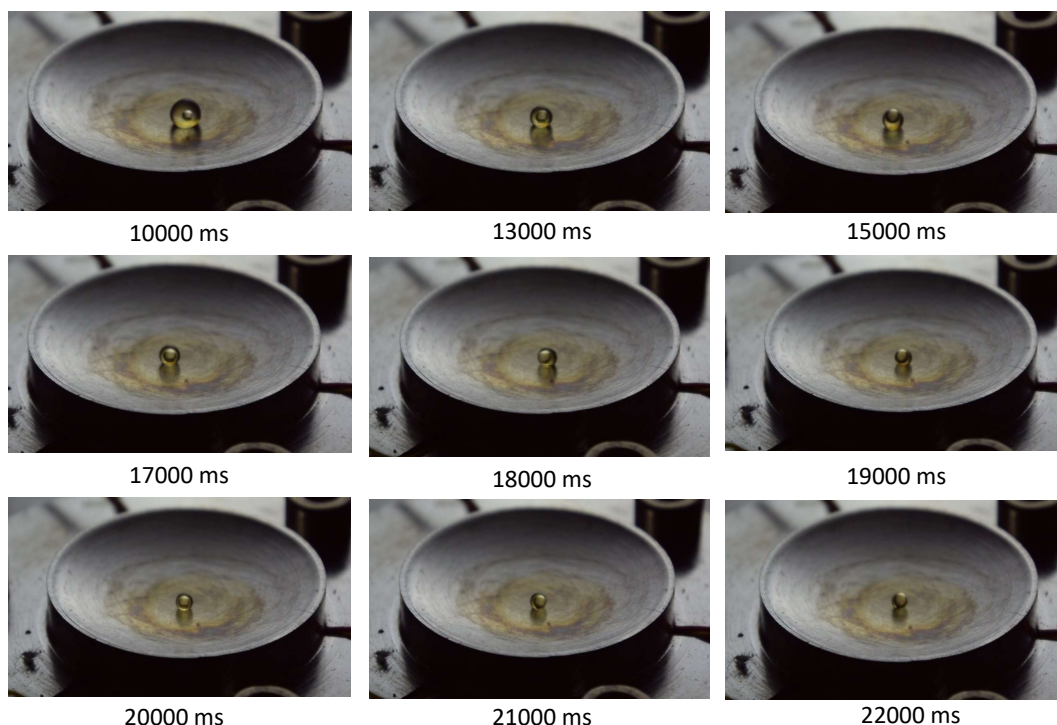


Figure 4.22: Frames taken from the test with gasoline on the aluminum surface under film boiling conditions.

It is possible to verify that during its evaporation process, a bubble vapor is forming inside the droplet along the evaporation process. Through the analysis of the videos, was possible to verify that, the droplet explodes when its radius coincides with the bubble vapor radius. This phenomenon occurred randomly during the tests with pure gasoline and gasoline-ethanol blends. Perhaps this phenomenon explains why Leidenfrost temperatures for these fluids were not possible to be obtained.

## 4.6 Weber number influence on the Nukiyama and Leidenfrost temperatures

The Figure 4.23 shows the result of the droplet impact test on a heated copper surface, where n-heptane was used as the test fluid. The objective of this investigation was to evaluate the influence of Weber number on the nucleate boiling regime, Nukiyama point, transition region, Leidenfrost point and film boiling regime. To calculate the parameters, the Equation. D.1 and 2.19 were used and assumed that droplet released by the syringe has a spherical shape. Through the Figure. 4.23, it is possible to conclude that the Weber number does not influence significantly in the nucleate boiling region, however, the transition regime, Leidenfrost point, and film boiling regime are affected by the parameter studied.

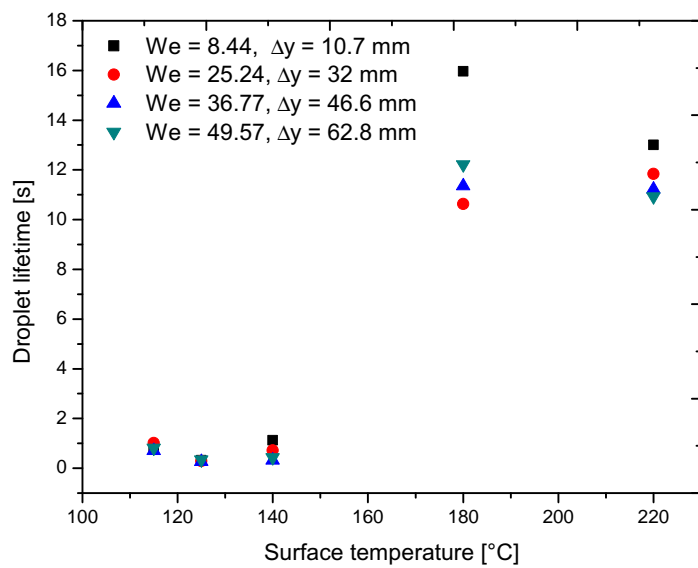


Figure 4.23: Results of the impact test for n-heptane for different Weber numbers.

Another test was conducted in order to verify the influence of the oxide layer formed on the surface of the test section in the cited above boiling regimes. Comparing the results the results of Figure 4.24, it was concluded that the oxide layer influences the results obtained in the boiling regime in the transition (temperature corresponds to 140°C) and Leidenfrost point (180°C).

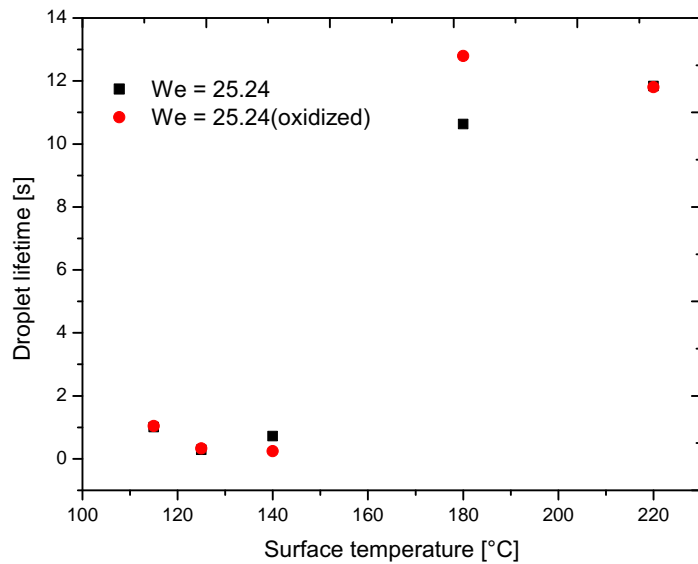


Figure 4.24: Results of the impact test for n-Heptane with an oxide layer formed on the test section surface for different Weber numbers.

Figure 4.25 shows some frames of the n-heptane evaporation phenomenon on a copper surface with a temperature of 180°C (Leidenfrost temperature) in different Weber numbers.



Figure 4.25: Outcome of n-heptane droplet impacting on a heated copper surface for different Weber numbers.

It is noted that as the Weber number is increased the n-heptane droplet experiences different behaviors when in contact with the heating surface. These behaviors were explained previously in section 2. Weber number of 8.44 the droplet is gently deposited on the copper surface. With the increase of We to 25.4 when coming into contact with the surface the droplet

spreads. For  $We = 36.77$  the droplet suffers the phenomenon of prompt splash where the droplet spreads on the surface and returns to its original shape. For the number of  $We = 49.57$ , the droplet spreads abruptly on the surface (splash) and fragments into droplets.

## 5 CONCLUSION

### 5.1 Summary

The objective of this research was using the droplet evaporation method onto a heated surface to identify the Nukiyama and Leidenfrost temperature for single-components and binary mixtures. Experimental results obtained through the tests were compared with other experimental data, and values calculated by correlations and models available in the literature. Surface material and Weber number influence on these critical temperatures was also investigated.

Nukiyama temperature in all single-components were found more precisely than Leidenfrost temperature. In the film boiling regime the characterization of the Leidenfrost temperature is more complex due to experimental limitation. Iso-octane and n-heptane showed some degree of similarity at the Nukiyama and Leidenfrost temperatures. One possible explanation for this behavior is the fact these hydrocarbons have similar physical-chemical properties.

In the experiments performed with ethanol and n-heptane mixture it is evident that the Nukiyama temperature decreased with the higher ethanol concentration. In relation to the Leidenfrost point, it is not possible to conclude something consistent.

The Nukiyama temperature was well characterized for gasoline-ethanol blends. It was observed that the Nukiyama point decreases as the ethanol composition increases in the blend. On the other hand, it was difficult to characterize the Leidenfrost temperature for most of this mixtures due to the experimental points show very close values.

Through this work it was possible to conclude that the Nukiyama and Leidenfrost points and even the transition boiling region can be influenced by the type of material of the heating surface. This influence is more significant in the Leidenfrost region as seen in the results presented in the previous section.

The Weber number did not show any significant influence at the temperature corresponding to the Nukiyama point, however, at the Leidenfrost point, this parameter cannot be neglected. Another important point was the difficulty of comparing the results of mixtures with correlations. The droplet evaporation method, besides being simple, proved to be efficient to find the Nukiyama and Leidenfrost temperatures for single-components.

## 5.2 Further work

- To test more binary mixtures of the ethanol and n-heptane compositions and other mixtures, in order to obtain a better understanding of the mixtures evaporation;
- Conduct further tests with gasoline-ethanol blends for a better clarification on the phenomena involved during its evaporation, and the difficulty in determining the Leidenfrost point;
- Predict the critical heat flux (CHF) taking into account the contact angle, and compare the values found with the correlations already tested.
- Investigate with more detail the influence of the heating surface material at the Nukiyama and Leidenfrost point;
- It is expected in future work to compare these results with other works and correlations existing in the literature;
- Suggested to more detailed investigations about the effect of wall material type, surface roughness, and oxidation.
- Carry out improvements in the experimental apparatus, as to encapsulate workbench to control the pressure and temperature conditions.

## References

- APLINC, J. Leidenfrost effect: drop on hot surfaces. In **Seminar in University of Ljubljana**. 2012.
- BAUMEISTER, K. and SIMON, F. Leidenfrost temperature—its correlation for liquid metals, cryogens, hydrocarbons, and water. **Journal of Heat Transfer**, v. 95, n. 2, 166–173, 1973.
- BAUMEISTER, K.J.; HENRY, R. and SIMON, F. Role of the surface in the measurement of the leidenfrost temperature. 1970.
- BAYER, I.S. and MEGARIDIS, C.M. Contact angle dynamics in droplets impacting on flat surfaces with different wetting characteristics. **Journal of Fluid Mechanics**, v. 558, 415–449, 2006.
- BERNARDIN, J. and MUDAWAR, I. The leidenfrost point: experimental study and assessment of existing models. **Transactions-American Society of Mechanical Engineers Journal of Heat Transfer**, v. 121, 894–903, 1999.
- BERTOLA, V. An impact regime map for water drops impacting on heated surfaces. **International Journal of Heat and Mass Transfer**, v. 85, 430–437, 2015.
- BIANCE, A.L.; CLANET, C. and QUÉRÉ, D. Leidenfrost drops. **Physics of Fluids**, v. 15, n. 6, 1632–1637, 2003.
- BRACCO, G. and HOLST, B. **Surface science techniques**. Springer Science & Business Media, 2013.
- BRUTIN, D. **Droplet wetting and evaporation: from pure to complex fluids**. Academic Press, 2015.
- CENGEL, Y.A. and CIMBALA, J.M. **Mecânica dos fluidos-3**. AMGH Editora, 2015.
- CHANG, J. and YOU, S. Heater orientation effects on pool boiling of micro-porous-enhanced

surfaces in saturated fc-72. **Journal of Heat Transfer**, v. 118, n. 4, 937–943, 1996.

CHAU, T. A review of techniques for measurement of contact angles and their applicability on mineral surfaces. **Minerals Engineering**, v. 22, n. 3, 213–219, 2009.

CHU, K.H.; SOO JOUNG, Y.; ENRIGHT, R.; BUIE, C.R. and WANG, E.N. Hierarchically structured surfaces for boiling critical heat flux enhancement. **Applied Physics Letters**, v. 102, n. 15, 151602, 2013.

COOPER, M. Heat flow rates in saturated nucleate pool boiling-a wide-ranging examination using reduced properties. In **Advances in heat transfer**, v. 16, pp. 157–239. Elsevier, 1984.

COSSALI, G.; MARENKO, M. and SANTINI, M. Multiple drop impact on heated surface. **Proceedings of the 9th ICLASS, Sorrento, Italy**, 2003.

DAS, S.; KUMAR, D. and BHAUMIK, S. Experimental study of nucleate pool boiling heat transfer of water on silicon oxide nanoparticle coated copper heating surface. **Applied Thermal Engineering**, v. 96, 555–567, 2016.

DAS, S.; SAHA, B. and BHAUMIK, S. Experimental study of nucleate pool boiling heat transfer of water by surface functionalization with sio<sub>2</sub> nanostructure. **Experimental Thermal and Fluid Science**, v. 81, 454–465, 2017.

DELLA VOLPE, C.; MANIGLIO, D.; MORRA, M. and SIBONI, S. The determination of a ‘stable-equilibrium’ contact angle on heterogeneous and rough surfaces. **Colloids and Surfaces A: Physicochemical and Engineering Aspects**, v. 206, n. 1-3, 47–67, 2002.

DHILLON, N.S.; BUONGIORNO, J. and VARANASI, K.K. Critical heat flux maxima during boiling crisis on textured surfaces. **Nature communications**, v. 6, 8247, 2015.

FANG, X.; PIMENTEL, M.; SOKOLOV, J. and RAFAILOVICH, M. Dewetting of the three-phase contact line on solids. **Langmuir**, v. 26, n. 11, 7682–7685, 2010.

FARDAD, D. and LADOMMATOS, N. Evaporation of hydrocarbon compounds, including gasoline and diesel fuel, on heated metal surfaces. **Proceedings of the Institution of Mechanical Engineers, Part D: Journal of Automobile Engineering**, v. 213, n. 6, 625–645, 1999.

GAJEWSKI, A. Contact angle and sessile drop diameter hysteresis on metal surfaces. **International Journal of Heat and Mass Transfer**, v. 51, n. 19-20, 4628–4636, 2008.

GORENFLO, D.; LUKE, A.; KÜNSTLER, W. and BUSCHMEIER, M. Prediction of pool boiling heat transfer with new refrigerants. **Cfc's the day after, Padova, spt**, pp. 21–23, 1994.

HABCHI, C. A comprehensive model for liquid film boiling in internal combustion engines. **Oil & Gas Science and Technology–Revue de l'Institut Français du Pétrole**, v. 65, n. 2, 331–343, 2010.

HSU, C.C. and CHEN, P.H. Surface wettability effects on critical heat flux of boiling heat transfer using nanoparticle coatings. **International Journal of Heat and Mass Transfer**, v. 55, n. 13-14, 3713–3719, 2012.

HSU, H.Y.; LIN, M.C.; POPOVIC, B.; LIN, C.R. and PATANKAR, N.A. A numerical investigation of the effect of surface wettability on the boiling curve. **PloS one**, v. 12, n. 11, e0187175, 2017.

JO, H.; AHN, H.S.; KANG, S. and KIM, M.H. A study of nucleate boiling heat transfer on hydrophilic, hydrophobic and heterogeneous wetting surfaces. **International Journal of Heat and Mass Transfer**, v. 54, n. 25-26, 5643–5652, 2011.

KANDLIKAR, S.G. A theoretical model to predict pool boiling chf incorporating effects of contact angle and orientation. **Journal of Heat Transfer**, v. 123, n. 6, 1071–1079, 2001.

KHAVARI, M.; SUN, C.; LOHSE, D. and TRAN, T. Fingering patterns during droplet impact on heated surfaces. **Soft Matter**, v. 11, n. 17, 3298–3303, 2015.

KIM, J.; JUN, S.; LAKSNARAIN, R. and YOU, S.M. Effect of surface roughness on pool boiling heat transfer at a heated surface having moderate wettability. **International Journal of Heat and Mass Transfer**, v. 101, 992–1002, 2016.

KIM, Y.C. Evaporation of nanofluid droplet on heated surface. **Advances in Mechanical Engineering**, v. 7, n. 4, 1687814015578358, 2015.

KUBIAK, K.; WILSON, M.; MATHIA, T. and CARVAL, P. Wettability versus roughness of

engineering surfaces. **Wear**, v. 271, n. 3-4, 523–528, 2011.

KUTATELADZE, S. Hydromechanical model of heat transfer crisis in pool liquid boiling. **J. Tech. Phys.**, v. 20, n. 11, 1389–1392, 1950.

KWOK, D.Y. and NEUMANN, A.W. Contact angle measurement and contact angle interpretation. **Advances in colloid and interface science**, v. 81, n. 3, 167–249, 1999.

LI, R. and HUANG, Z. A new chf model for enhanced pool boiling heat transfer on surfaces with micro-scale roughness. **International Journal of Heat and Mass Transfer**, v. 109, 1084–1093, 2017.

LIANG, G. and MUDAWAR, I. Pool boiling critical heat flux (chf)—part 2: Assessment of models and correlations. **International Journal of Heat and Mass Transfer**, 2017a.

LIANG, G. and MUDAWAR, I. Review of drop impact on heated walls. **International Journal of Heat and Mass Transfer**, v. 106, 103–126, 2017b.

LIAO, L.; BAO, R. and LIU, Z. Compositive effects of orientation and contact angle on critical heat flux in pool boiling of water. **Heat and Mass Transfer**, v. 44, n. 12, 1447–1453, 2008.

LIENHARD, J.; DHIR, V. and RIHERD, D. Peak pool boiling heat-flux measurements on finite horizontal flat plates. **Journal of Heat Transfer**, v. 95, n. 4, 477–482, 1973.

MAHULKAR, A.V.; MARIN, G.B. and HEYNDERICKX, G.J. Droplet–wall interaction upon impingement of heavy hydrocarbon droplets on a heated wall. **Chemical Engineering Science**, v. 130, 275–289, 2015.

MANZELLO, S.L. and YANG, J.C. On the collision dynamics of a water droplet containing an additive on a heated solid surface. In **Proceedings of the Royal Society of London A: Mathematical, Physical and Engineering Sciences**, v. 458, pp. 2417–2444. The Royal Society, 2002.

MARMUR, A. Soft contact: measurement and interpretation of contact angles. **Soft Matter**, v. 2, n. 1, 12–17, 2006.

MARMUR, A. Solid-surface characterization by wetting. **Annual Review of materials research**, v. 39, 473–489, 2009.

MEYER, J.H. Manual on the use of thermocouples in temperature measurement. 1982.

MILLS, A. and SHARROCK, N. Rate of evaporation of n-alcohols from a hot surface: Nukiyama and leidenfrost temperatures. **European Journal of Physics**, v. 7, n. 1, 52, 1986.

MISYURA, S. Wall effect on heat transfer crisis. **Experimental Thermal and Fluid Science**, v. 70, 389–396, 2016.

MOREIRA, A.; MOITA, A. and PANAO, M. Advances and challenges in explaining fuel spray impingement: How much of single droplet impact research is useful? **Progress in energy and combustion science**, v. 36, n. 5, 554–580, 2010.

MORI, S. and UAKA, Y. Critical heat flux enhancement by surface modification in a saturated pool boiling: a review. **International Journal of Heat and Mass Transfer**, v. 108, 2534–2557, 2017.

MUDAWAR, I.; HOWARD, A.H. and GERSEY, C.O. An analytical model for near-saturated pool boiling critical heat flux on vertical surfaces. **International journal of heat and mass transfer**, v. 40, n. 10, 2327–2339, 1997.

NAIR, H.; STAAT, H.J.; TRAN, T.; VAN HOUSELT, A.; PROSPERETTI, A.; LOHSE, D. and SUN, C. The leidenfrost temperature increase for impacting droplets on carbon-nanofiber surfaces. **Soft matter**, v. 10, n. 13, 2102–2109, 2014.

NAKORYAKOV, V.; MISYURA, S.Y. and ELISTRATOV, S. The behavior of water droplets on the heated surface. **International Journal of Heat and Mass Transfer**, v. 55, n. 23-24, 6609–6617, 2012.

NAKORYAKOV, V.; MISYURA, S.Y. and ELISTRATOV, S. Boiling crisis in droplets of ethanol water solution on the heating surface. **Journal of Engineering Thermophysics**, v. 22, n. 1, 1–7, 2013.

NEGEED, E.S.R.; ALBEIRUTTY, M.; AL-SHARIF, S.F.; HIDAKA, S. and TAKATA, Y. Dy-

namic behavior of a small water droplet impact onto a heated hydrophilic surface. **Journal of Heat Transfer**, v. 138, n. 4, 042901, 2016.

OLIVEIRA, A.V.; MEDEIROS FILHO, D.L. and DOS SANTOS, R.G. Determination of boiling critical temperatures of pure and binary mixtures of water and ethanol by droplet evaporation. **IV Journeys in Multiphase Flows (JEM2015)**, 2015.

PEYGHAMBARZADEH, S.; JAMILAHMADI, M.; ALAVI FAZEL, S. and AZIZI, S. Experimental and theoretical study of pool boiling heat transfer to amine solutions. **Brazilian Journal of Chemical Engineering**, v. 26, n. 1, 33–43, 2009.

POLING, B.; PRAUSNITZ, J. and O'CONNELL, J. **The Properties of Gases and Liquids**. McGraw-Hill, 5<sup>th</sup> ed., 2001.

QUÉRÉ, D. Wetting and roughness. **Annu. Rev. Mater. Res.**, v. 38, 71–99, 2008.

RAHMAN, M.M.; OLCEROGLU, E. and MCCARTHY, M. Role of wickability on the critical heat flux of structured superhydrophilic surfaces. **Langmuir**, v. 30, n. 37, 11225–11234, 2014.

REIN, M. **Drop-surface interactions**, v. 456. Springer, 2002.

RIBATSKI, G. and JABARDO, J.M.S. Experimental study of nucleate boiling of halocarbon refrigerants on cylindrical surfaces. **International journal of heat and mass transfer**, v. 46, n. 23, 4439–4451, 2003.

RIOBOO, R.; TROPEA, C. and MARENKO, M. Outcomes from a drop impact on solid surfaces. **Atomization and Sprays**, v. 11, n. 2, 2001.

SEGAWA, D.; KADOTA, T.; NAKAYA, S.; TAKEMURA, K. and SASAKI, T. A liquid film or droplet of miscible binary fuel burning on a heated surface at elevated pressures. **Proceedings of the Combustion Institute**, v. 32, n. 2, 2187–2194, 2009.

SERAJ, M.M. and GADALA, M.S. Wetting front propagation during quenching of aluminum plate by water spray. **International Journal of Mechanical, Aerospace, Industrial, Mechatronic and Manufacturing Engineering**, v. 7, n. 6, 1151 – 1155, 2013.

SOMEYA, S.; YOSHIDA, S.; OKAMOTO, K.; LI, Y.R.; TANGE, M. and UDDIN, M.M. Jet ejection from droplets near the leidenfrost temperature. **Journal of visualization**, v. 13, n. 1, 41–47, 2010.

SPIEGLER, P.; HOPENFELD, J.; SILBERBERG, M.; BUMPUS, C. and NORMAN, A. Onset of stable film boiling and the foam limit. **International Journal of Heat and Mass Transfer**, v. 6, n. 11, 987–989, 1963.

STANGLMAIER, R.H.; ROBERTS, C.E. and MOSES, C.A. Vaporization of individual fuel drops on a heated surface: A study of fuel-wall interactions within direct-injected gasoline (dig) engines. Relatório técnico, SAE Technical Paper, 2002.

STEPHAN, K. and ABDELSALAM, M. Heat-transfer correlations for natural convection boiling. **International Journal of Heat and Mass Transfer**, v. 23, n. 1, 73–87, 1980.

TALARI, V.; BEHAR, P.; LU, Y.; HARYADI, E. and LIU, D. Leidenfrost drops on micro-/nanostructured surfaces. **Frontiers in Energy**, pp. 1–21, 2018.

THEOFANOUS, T.; TU, J.; DINH, A. and DINH, T.N. The boiling crisis phenomenon: Part i: nucleation and nucleate boiling heat transfer. **Experimental thermal and fluid science**, v. 26, n. 6-7, 775–792, 2002.

VISHNEV, I. Effect of orienting the hot surface with respect to the gravitational field on the critical nucleate boiling of a liquid. **Journal of engineering physics**, v. 24, n. 1, 43–48, 1973.

WANG, A.B.; LIN, C.H. and CHEN, C.C. The critical temperature of dry impact for tiny droplet impinging on a heated surface. **Physics of Fluids**, v. 12, n. 6, 1622–1625, 2000.

WENZEL, R.N. Resistance of solid surfaces to wetting by water. **Industrial & Engineering Chemistry**, v. 28, n. 8, 988–994, 1936.

XIONG, T. and YUEN, M. Evaporation of a liquid droplet on a hot plate. **International journal of heat and mass transfer**, v. 34, n. 7, 1881–1894, 1991.

YAGOV, V.V. Is a crisis in pool boiling actually a hydrodynamic phenomenon? **International Journal of Heat and Mass Transfer**, v. 73, 265–273, 2014.

YAWS, C.L. **Thermophysical properties of chemicals and hydrocarbons**. William Andrew, 2008.

ZHONG, L. and GUO, Z. Effect of surface topography and wettability on the leidenfrost effect. **Nanoscale**, v. 9, n. 19, 6219–6236, 2017.

ZUBER, N. On the stability of boiling heat transfer. **Trans. Am. Soc. Mech. Engrs.**, v. 80, 1958.

## APPENDIX A – Calibration curves and uncertainties analysis

### A.1 Calibration curve for the copper surface

Figures A.1 to A.3, show the curves created from the experimental points obtained during the calibration tests for the copper surface used to make the adjustments in the experimental data.

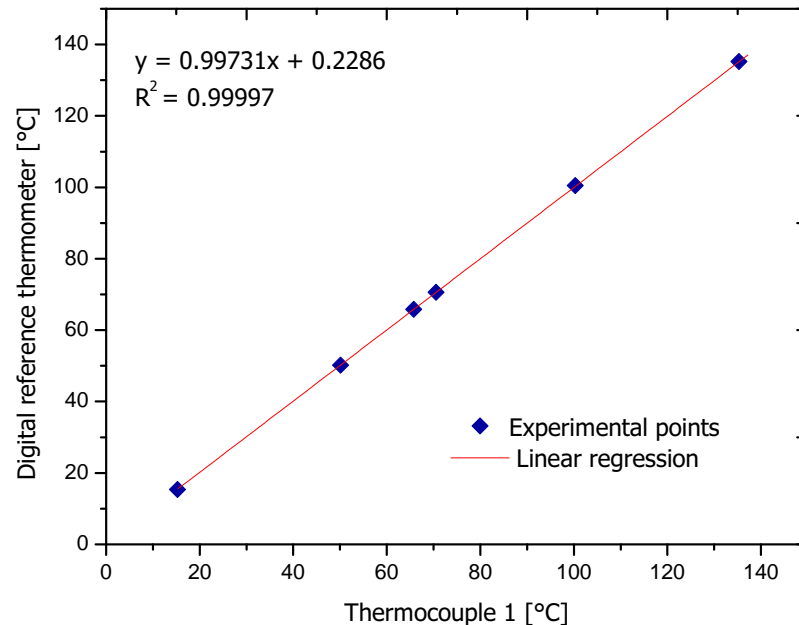


Figure A.1: Curve calibration for thermocouple 1.

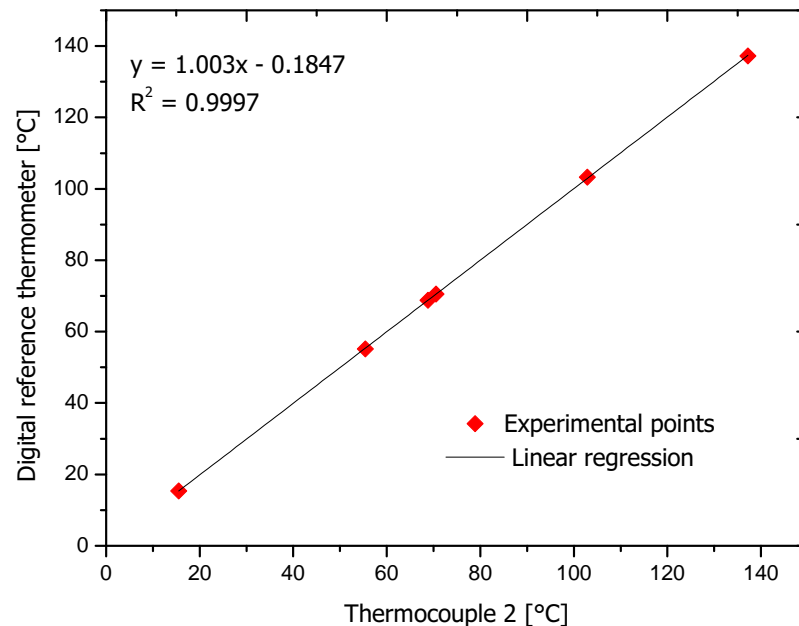


Figure A.2: Curve calibration for thermocouple 2.

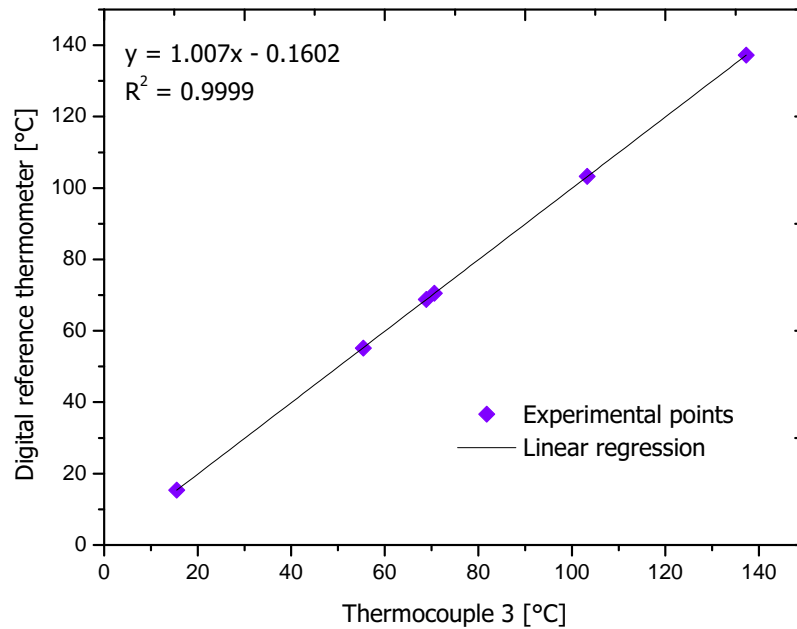


Figure A.3: Curve calibration for thermocouple 3.

## A.2 Calibration curve for the aluminum surface

Figures A.4 to A.6, show the curves created from the experimental points obtained during the calibration tests for the aluminum surface.

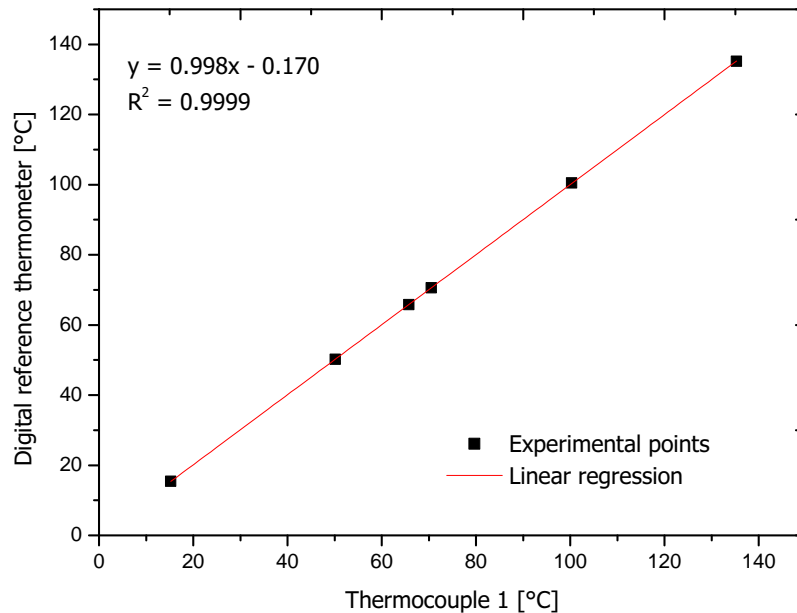


Figure A.4: Curve calibration for thermocouple 1.

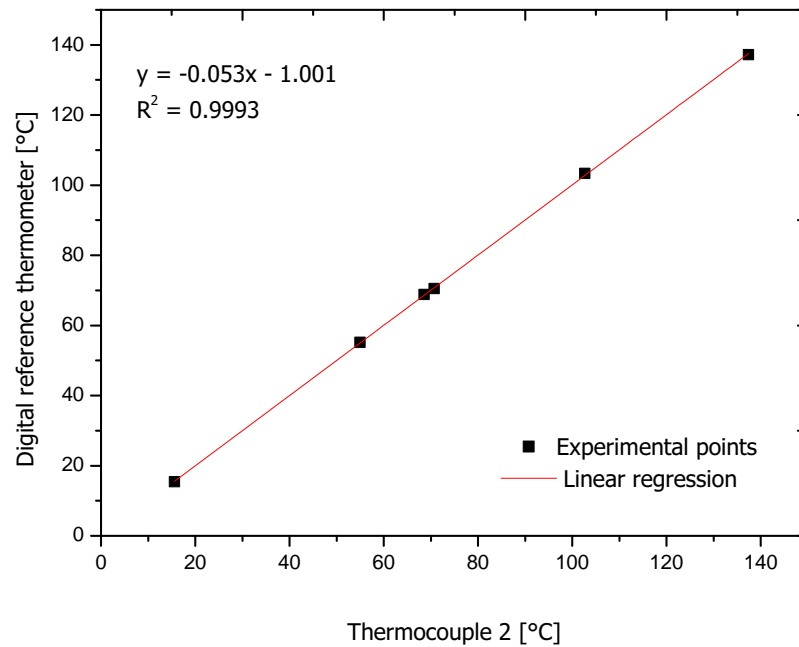


Figure A.5: Curve calibration for thermocouple 2.

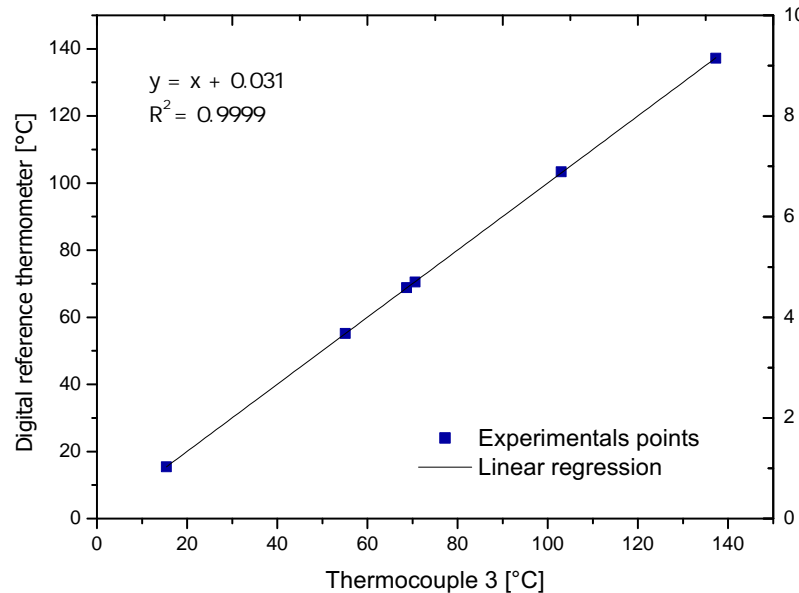


Figure A.6: Curve calibration for thermocouple 3.

### A.3 Uncertainties analysis

#### A.3.1 Test section temperature and digital camera

In this section presented the main errors present in the measuring instruments as inherent errors of thermocouples. These sensors were calibrated in a temperature range between 15°C to 137°C. Considering a standard deviation of 0.74 and a t-student ( $t = 3.3$ ) and a reliability of

99.9. Experimental temperature uncertainty was  $\pm 0.24^{\circ}\text{C}$  for thermocouples and  $\pm 0.016\text{ s}$  for digital camera.

## APPENDIX B – Properties of test fluids and heating surface

### B.1 Test fluid properties

Table B.1: Thermophysical properties of tested fluids (Fardad and Ladommatos, 1999, Poling *et al.*, 2001 and Yaws, 2008)

Fluids	Density ( $kg/m^3$ )	Surface tension (N/m)	$T_{sat}$ (K)	$T_b$ (K)	$T_c$ (K)
Water	0.590	0.058	372.76	373.15	647.13
Ethanol	736.15	0.017	351.13	350.2	513.92
Iso-Octane	623.26	0.012	372	390.8	543.8
n-Heptane	614.64	0.013	614.64	371.53	540.2
Gasoline	750	0.002	310-477	374.15	—

### B.2 Heating surface properties

Table B.2: Thermal and physical properties of the wall material used in the tests at 127°C (Misyura, 2016).

Thermophysical properties	Copper	Aluminum
Thermal conductivity ( $W/(m \cdot K)$ )	392	239
Density ( $kg/m^3$ )	8870	2675
Heat capacity ( $J/(kg \cdot K)$ )	389	951
Thermal difusivity ( $m^2/s$ )	$111 \cdot 10^{-6}$	$94 \cdot 10^{-6}$

## APPENDIX C – Contact angle

Figure. C.1 shows an experimental apparatus used to measure the contact angle. The contact angle measurement was carried out by depositing the test fluids onto a surface. When deposited, it is expected that droplet enters into balance in which is recorded through photography. These images aid in measuring the contact angle that is made via software.



Figure C.1: Experimental apparatus used for contact angle measurement (University of Sao Paulo).

The tested fluids are shown in the Table. C.1.

Table C.1: Values obtained for contact angle at the copper (cu) and Aluminum (Al) surface.

Fluids	Contact angle (Cu)	Contact angle (Al)
Distilled water	66.709	77.254
Ethanol	5.524	6.272
Iso-Octane	7.144	8.325
n-Heptane	6.230	7.970
Gasoline	—	—

Through the table it is possible to verify that the distilled water has a high contact angle in relation to the other fluids and the gasoline contact can not be measured due to its high wettability degree (see Figure. C.2). It is also possible to notice that the contact angle values for these fluids have lower values for copper surface than aluminum surface. This shows how the same fluids can vary its wettability on different surfaces.

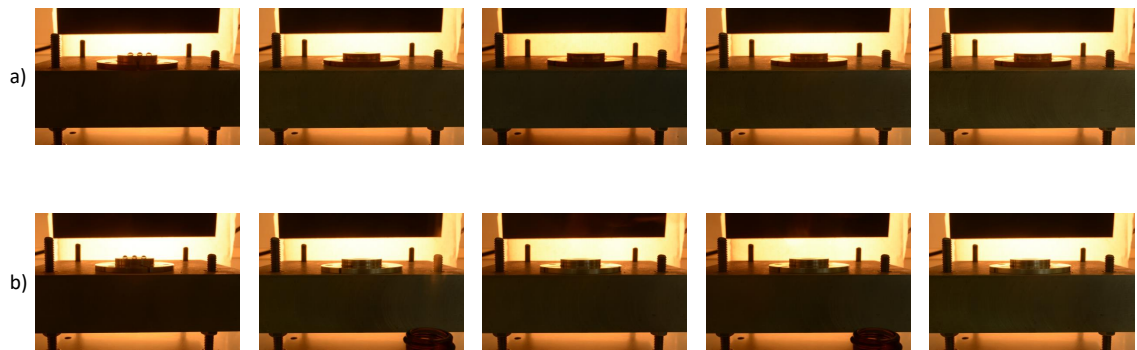


Figure C.2: Contact angle for single-components on the copper surface (a) and at the aluminum surface (b).

## APPENDIX D – Impact velocity

### D.1 Influence of the air resistance force in the droplet

The objective of calculating the droplet impact velocity on a solid surface using the models and the Torricelli equation (cited in 2.5) is to evaluate the influence of the resistance during droplet falling. The equations used to calculate the droplet impact velocity on a heated surface were:

- Torricelli equation;

$$u_0 = \sqrt{2g\Delta y} \quad (\text{D.1})$$

This equation neglecting the friction and viscosity.

- Model proposed by the present author;

The proposal was created a model from the equation of motion for the droplet after its separation from the needle. In this model, some hypotheses have been considered as droplet with the spherical shape and the only forces that act are weight and the air resistance force.

$$\sum F_y = ma_y = m \frac{du}{dt} \quad (\text{D.2})$$

$$\sum F_y = m \frac{du}{dy} \frac{dy}{dt} = mu \frac{du}{dy} \quad (\text{D.3})$$

$$\sum F_y = F_D - mg = ku^2 - mg = mu \frac{du}{dy} \quad (\text{D.4})$$

$$\int_0^y dy = \int_0^u \frac{mudu}{ku^2 - mg} \quad (\text{D.5})$$

integrating this expression, applying logarithm and solving for  $u$  results in:

$$u_1 = \left( \frac{mg}{k} \left( 1 - e^{[(2k/m)h]} \right) \right)^{1/2} \quad (\text{D.6})$$

where:

$$y - y_0 = h \quad (\text{D.7})$$

The parameter  $k$  is given by:

$$k = \frac{C_D A \rho}{2} \quad (\text{D.8})$$

where  $g$  is gravitational force, and  $m$ ,  $D_0$ ,  $A$ ,  $h$ ,  $C_D$ ,  $\rho$  are: gravity, droplet mass, droplet diameter area, droplet falling height, drag coefficient, mass density, respectively. The drag coefficient ( $C_D$ ) was considered as 0.4 (Cengel and Cimbala, 2015) assuming that the droplet has a spher-

ical shape during its fall.

Table. D.1 shows the comparison of droplet impact velocity values through of the equations presented in section 2

Table D.1: Values obtained for droplet impact velocity.

Height (mm)	$u_0$ (m/s)	$u_1$ (m/s)
10.7	0.458	0.453
32.0	0.798	0.778
46.6	0.956	0.934
62.8	1.110	1.071

Observing the results obtained through these equations (Tab. D.1), it is possible to notice that the velocity values calculated by the Torricelli equation ( $u_0$ ) begin to present a significant difference in relation to the Equation. D.6 as the height of droplet release is increased. Therefore, as all evaporation tests were performed at a 10.7 mm height, the drag effect can be neglected.

## APPENDIX E – Needle's temperature

### E.1 Influence of the thermal radiation induced by high temperature of the tests section on the needle's temperature

Initially, the needle warm-up was investigated as a function of time. The test consisted of keeping the needle at a distance of 10.7 mm from the test section with a temperature set at 250°C during 5 minutes. This distance corresponds to the height at which the needle is held in relation to the heated surface for the launch of the droplet. As observed (Fig. E.1), from 7 seconds its temperature increased by 1°C. It was important to evaluate this parameter because the droplet launch on the surface had a duration of approximately 5 seconds, thereafter, the needle is immediately spaced far from the surface.

It can be concluded that, the fluid contained in the syringe does not suffer much influence of the radiation emitted by the copper dish during the experiments.

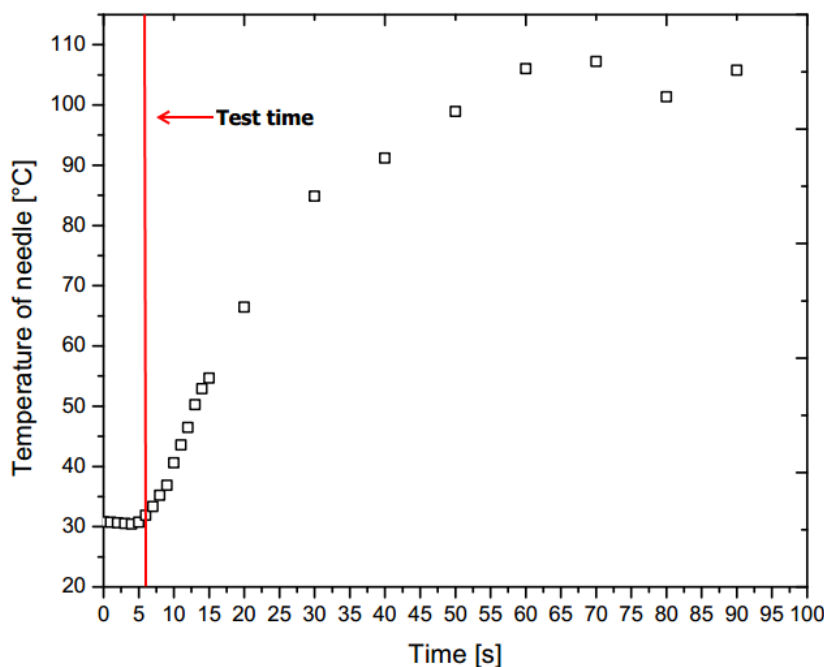


Figure E.1: Needle temperature variation with time (test section at 250°C)

## APPENDIX F – Pneumatic system code

```

int stateboot1 = 0; // ---- Button state gets 0.
int stateboot2 = 0; // ---- Button state gets 0.
int stateboot3 = 0; // ---- Button state gets 0.

int passogota = 10; // ---- Qty of steps
//in the clockwise direction

int red = 4; // ---- Pin 4 for the red LED.
int ledverde = 5; // ---- Pin 5 for the green LED.
int ledamarelo = 6; // ---- Pin 6 for the yellow LED.
int acionamentopneu = 7; // ---- Pin 7 for pneumatic
//valve actuation.

const int PassesPorRevolucao = 2048; // Total quantities
// of steps for a complete revolution.

// PIN INITIATION FOR 8-11 ENGINE
// Stepper myStepper (Steps forRevolution, 8,9,10,11);

Stepper motor (Steps for Replenishment, 8,9,10,11);

// =====
// PIN STATUS
void setup () {
pinMode (liberagota, INPUT_PULLUP);
pinMode (return, INPUT_PULLUP);
pinMode (forward, INPUT_PULLUP);
pinMode (on / off, OUTPUT);
pinMode (red led, OUTPUT);
pinMode (green led, OUTPUT);
pinMode (yellow LED, OUTPUT);
// TURN ON ALL LED'S FOR 2 SECONDS
digitalWrite (led red, HIGH);
digitalWrite (ledverde, HIGH);
digitalWrite (yellow LED, HIGH);

delay (2000);
}

```

```
// DELETE THE GREEN AND YELLOW LED'S
digitalWrite (ledverde, LOW);
digitalWrite (yellow, LOW);

// BOOT SPEED 6 rpm:
// myStepper.setSpeed(6);
motor.setSpeed(6);
// SERIAL PORT INITIALIZATION:
Serial.begin (9600);
}

void loop () {
// =====// RED BUTTON OPERATION =====
//RETURN
// LIFTING THE BOTTLE:

statusboot1 = digitalRead (return);
if (stateboot1 == 0) {
digitalWrite (yellow LED, HIGH);
digitalWrite (ledverde, LOW);
digitalWrite (led red, LOW);
delay (1000);
for (j = 1; j <= 10; j++)
Serial.println ("RETURN");
motor.step (Steps forRevolution);
// digitalWrite (red led, HIGH);
// digitalWrite (yellow, LOW);
// digitalWrite (triggered, LOW);
statusboot1 = digitalRead (return);
if (stateboot1 == 0) {
digitalWrite (led red, HIGH);
digitalWrite (yellow, LOW);
delay (500);
break;
}
}
} // END RETURN
// =====
```

```
// DRIVING THE GREEN BOOT

// Step to release droplet

statusbotao2 = digitalRead (liberagota);

if (stateboot2 == 0) {

    digitalWrite (yellow, LOW);
    digitalWrite (ledverde, HIGH);
    digitalWrite (led red, LOW);

    for (i = 1; i <= 100; i++)
        if (digitalRead (liberagota) == 0) {
            if (i == 100) {
                digitalWrite (yellow, LOW);
                digitalWrite (ledverde, HIGH);
                digitalWrite (led red, LOW);
                while (digitalRead (liberagota) == 0) {
                    Serial.println ("AVANCO");
                    motor.step (passogota);
                }
            }
        }

    delay (10);

}

delay (500);
digitalWrite (on-the-fly, LOW);
digitalWrite (led red, HIGH);
digitalWrite (ledverde, LOW);

} // End if
```

```
// ======

// RED BOOT OPERATION

// Move down mechanism

statusboot3 = digitalRead (forward);

if (stateboot3 == 0) {



digitalWrite (yellow, LOW);
digitalWrite (ledverde, HIGH);
digitalWrite (led red, LOW);

delay (1000);
digitalWrite (high-pitched, HIGH);


} // ===== End if ======
} // =====End loop ======
```